

**INVESTIGATING THE ELECTROCHEMICAL PROPERTIES OF A
NEWLY DEVELOPED FE-CR ALLOY (FE-18CR-XSI) WITH
SILICON ADDITION**

BY

NABEEL AMEER

A Thesis Presented to the
DEANSHIP OF GRADUATE STUDIES

KING FAHD UNIVERSITY OF PETROLEUM & MINERALS

DHAHRAN, SAUDI ARABIA

In Partial Fulfillment of the
Requirements for the Degree of

MASTER OF SCIENCE

In

MATERIAL SCIENCE & ENGINEERING

DECEMBER 2017

KING FAHD UNIVERSITY OF PETROLEUM & MINERALS


DHAHRAN- 31261, SAUDI ARABIA

DEANSHIP OF GRADUATE STUDIES

This thesis, written by **NABEEL AMEER** under the direction of his thesis advisor and approved by his thesis committee, has been presented and accepted by the Dean of Graduate Studies, in partial fulfillment of the requirements for the degree of **MASTER OF SCIENCE IN MATERIALS SCIENCE & ENGINEERING**.



Dr. IHSAN-UL-HAQ TOOR
(Advisor)



Dr. ZUHAIR M. GASEM
Department Chairman



Dr. HASSAN M. BADR
(Member)



Dr. SALAM A. ZUMMO
Dean of Graduate Studies



Dr. M. ABDUL SAMAD
(Member)

15/5/16

Date

© Nabeel Ameer

2017

In the name of Allah, the Most Gracious, the Most Merciful. I would like to dedicate this thesis to my beloved parents and family for their support and encouragement |

ACKNOWLEDGMENTS

First of all, I would like to thank Almighty Allah for his blessings, guidance and help to complete this thesis. There are many people whom I have to acknowledge for their support so, I would like to take this opportunity to express my heartfelt gratitude to all those who helped me to make my thesis work a success.

I express my sincere and whole hearted thanks, to my Mentor / Advisor Dr. Ihsan-Ul - Haq Toor, Associate Professor, Department of Mechanical Engineering, for his regular advice, and his invaluable help of constructive comments and suggestions throughout the experimental work and thesis. I am highly indebted to his valuable support and patience which helped me to present this work in the right perspective. I am really indebted to him more than he knows. I express my deepest gratitude to my committee members, Dr. Hassan Badr and Dr. Abdul Samad for their support and knowledge regarding this topic.

Sincere thanks to all my friends from university and at my workplace, technical staff in the lab and others for their kindness and support. Thanks for the friendship.

Last but not the least, my deepest gratitude goes to my beloved parents; the ones who can never ever be thanked enough, for the overwhelming love and care they bestow upon me. Without their continuous moral and financial support and proper guidance it would have been impossible for me to complete my higher education.

TABLE OF CONTENTS

ACKNOWLEDGMENTS	III
TABLE OF CONTENTS	IV
LIST OF TABLES	VII
LIST OF FIGURES	VIII
LIST OF ABBREVIATIONS	XII
ABSTRACT	XIII
ملخص الرسالة	XV
CHAPTER 1 INTRODUCTION	1
1.1 Corrosion & Stainless Steels (SSs)	1
1.2 Passive Films on SSs	5
1.3 Types of SSs	7
1.4 Ferritic SSs	8
CHAPTER 2 LITERATURE REVIEW	9
2.1 Role of alloying elements and their characteristics	9
2.2 Alloy Development using Schaeffler Diagram	11
2.3 Role of Silicon(Si) Addition on the Corrsion Properties of Steels	13
2.4 Advanced Electrochemical Techniques for Corrosion Testing of SSs	24
2.5 Effect of Grain Size on Electrochemical Properties	28

CHAPTER 3 MOTIVATION AND OBJECTIVES OF THE RESEARCH.....	35
CHAPTER 4 MATERIALS AND METHODOLOGY	37
4.1 Alloy Development	37
4.2 Sample Characterization	38
4.3 Electrochemical Investigation	38
CHAPTER 5 RESULTS & DISCUSSION	40
5.1 Microstructural Examination	40
5.2 Identification of Chromium Carbide Formation	43
5.3 Localised Corrosion Behaviour of Fe-18Cr-XSi (X=0-4).....	46
5.3.1. Potentiodynamic Polarization (PDP) in 0.5M NaCl Solution.....	46
5.3.2. Potentiodynamic Polarization (PDP) in Acidic Chloride Solution 0.1M NaCl+0.1MH ₂ SO ₄	49
5.3.3. Electrochemical Impedance Spectroscopy (EIS) in Chloride Solution 0.5M NaCl.....	53
5.3.4. Electrochemical Impedance Spectroscopy (EIS) in Acidic Chloride Solution (0.1M NaCl+0.1MH ₂ SO ₄)	58
5.3.5. Linear Polarization Resistance (LPR)	60
5.4. Effect of Grain Size on Electrochemical Properties of Fe-18Cr-XSi Alloys	62
5.4.1. Effect of Grain Size on Localized Corrosion Resistance (Potentiodynamic Polarization Experiments)	62
5.4.2. Effect of Grain Size on Electrochemical Impedance Spectroscopy (EIS) Spectra in Chloride and Acidic Chloride Solution	67
CHAPTER 6 CONCLUSIONS	73

REFERENCES..... 74

VITAE..... 78

LIST OF TABLES

Table 1: Chemical Composition of Ferritic Stainless Steels Samples	37
Table 2: Summary of potentiodynamic polarization (PDP) experiments in 0.5MNaCl... 49	49
Table 3: Summary of potentiodynamic polarization (PDP) experiments in 0.5MNaCl and 0.1M NaCl+ 0.1M H ₂ SO ₄ solution for 30 min. annealed samples	52
Table 4: EIS parameters obtained in 0.5M NaCl solution for 30 min. annealed samples after curve fitting	58
Table 5: EIS parameters obtained in 0.1M NaCl + 0.1M H ₂ SO ₄ solution or 30 min. annealed samples after curve fitting	60
Table 6: LPR data in 0.5M NaCl & 0.1M NaCl+0.1M H ₂ SO ₄ solution for 30 min. Annealed samples	62
Table 7: Summary of potentiodynamic polarization (PDP) experiments in 0.5MNaCl solution for 30 and 60 min. annealed samples.....	65
Table 8: Combined potentiodynamic polarization (PDP) experimental data obtained in 0.5M NaCl & 0.1M NaCl+ 0.1M H ₂ SO ₄ solution for 30 & 60 min. annealed samples.....	67
Table 9: Combined EIS parameters obtained in 0.5M NaCl solution for 30 & 60 min. annealed samples after curve fitting	69
Table 10: Combined EIS parameters obtained in 0.1M NaCl+0.1M H ₂ SO ₄ solution for 30 & 60 min. annealed samples after curve fitting	72

LIST OF FIGURES

Figure 1: Binary iron-chromium equilibrium phase diagram [1]	3
Figure 2: Schematics of the Chromium Oxide (Cr_2O_3) present on SSs.....	4
Figure 3: Point defect model for generation and annihilation of cation vacancies [10]	6
Figure 4: Schaeffler diagram showing phases present in as- solidified stainless steels at room temperature [13]	12
Figure 5: Phase diagrams of Fe-Cr-Si ternary iron alloy [14]	14
Figure 6: Variation in weight with respect to time for samples Si1-Si5 with different silicon contents during isothermal oxidation at 800 °C [21].....	15
Figure 7: Variation in weight with respect to time for samples Si1-Si5 with different silicon contents during isothermal oxidation at 1000 °C [21].....	15
Figure 8: Potentiodynamic polarization spectra for sintered SSs in 3.5 wt.% NaCl solution a, IM 304L SS; b, PM 304L SS; c, PM 304L SS + 1 wt.% Si; d, PM 304L SS + 3wt% Si [22]	17
Figure 9: Potentiodynamic polarization spectra for sintered stainless steels in 6 wt.% FeCl_3 solution (pH 1.6) at 25 °C: a, IM 304L SS; b, PM 304L SS; c, PM 304L SS + 1 wt.% Si; d, PM 304L SS + 3wt% Si[22]	18
Figure 10: Polarization spectra of Powder Metallurgy SS after oxidation [23]	19
Figure 11: Potentiodynamic spectra obtained in 0.5 M H_2SO_4 at 25°C. Fe25Cr (○); Fe25Cr1Si (○); Fe25Cr3Si (▼); Fe25Cr5Si (□) [29]	21
Figure 12: Effect of Al and Mo on polarization spectra of Fe-10Cr-3Si 0.5M H_2SO_4 solution.[31]	23

Figure 13: AES Depth profile of passive films developed on Fe-10Cr-5Si by passivation in 30mass% HNO ₃ solution for 3.6ks [31].....	23
Figure 14: Schematic illustration of enrichment of Cr & Si in the passive film of Fe-10Cr-Si.[31]	24
Figure 15: Nyquist plot of the laser treated samples with equivalent circuit [45].....	26
Figure 16: Nyquist plots for 304L (O) and 316L (▲) Stainless steel in 5% NaCl [46] ..	26
Figure 17: Nyquist plots of CrAlSixN/AISI420 [47]	27
Figure 18: Nyquist plots of CrAlSixN/MS [47]	28
Figure 19: Microstructure of HN steel annealed at 900°C for 600s [59].....	29
Figure 20: Photomicrographs of Ferritic SS New obtained after annealing at different times at 1100 °C: (a) 0 min; (b) 5 min; (c) 10 min; (d) 30 min; (e) 60 min [61].....	31
Figure 21: Anodic polarization curves of Ferritic stainless steel samples with different annealing times in a 3.5 wt % NaCl solution.[61]	31
Figure 22: Photomicrographs of as-received and ECAPed 304 SS after different passes: (a) (0 pass), (b) 1 pass, (c) 4 pass (d) 8 pass [62].....	32
Figure 23: Potentiodynamic polarization curves of samples with and without ECAPed SS in 0.5 MH ₂ SO ₄ solution [62]	33
Figure 24: (a) Nyquist plots general and ECAPed samples and (b) magnified graph for the small black area in (a) [62]	34
Figure 25: Shows process flow chart for Fe-Cr alloy production.....	37
Figure 26: Schematic of polarization test apparatus (Potentiostat is connected with 3 electrode electrochemical cell).....	39

Figure 27: Microstructures of the alloys a) Fe-18Cr-0Si b) Fe-18Cr-2Si and c) Fe-18Cr-4Si annealed for 30 minutes	40
Figure 28: Microstructures of the alloys a) Fe-18Cr-0Si b) Fe-18Cr-2Si and c) Fe-18Cr-4Si annealed for 60 minutes	42
Figure 29: Sensitization curve of Ferritic & Austenitic SSs [66]	44
Figure 30: Steps between grains; Acceptable structure with no grain boundary carbides [63].....	45
Figure 31: Ditched structure; Unacceptable structure with grain boundary completely surrounded by carbides [63].....	45
Figure 32: Microstructures of the alloys a) Fe-18Cr-0Si b) Fe-18Cr-2Si and c) Fe-18Cr-4Si obtained after ASTM A763 (IGC) test. No ditches at grain boundaries were observed.....	46
Figure 33: Polarization curves obtained in 0.5M NaCl solution for 30minutes annealed samples.....	48
Figure 34: Polarization curves in 0.1M NaCl+ 0.1M H ₂ SO ₄ solution for 30minutes annealed samples	51
Figure 35: Nyquist plot in 0.5M NaCl solution for 30 minutes annealed samples.....	55
Figure 36: Bode plot in 0.5M NaCl solution for 30 minutes annealed samples	56
Figure 37: Two layered model used to fit the impedance curves of Fe-18Cr-XSi samples.....	57
Figure 38: Nyquist plot in 0.1M NaCl+ 0.1M H ₂ SO ₄ solution for 30 minutes annealed samples.....	59

Figure 39: Bode plot in 0.1M NaCl+ 0.1M H ₂ SO ₄ solution for 30 minutes annealed samples.....	60
Figure 40: Combined Polarization curves in 0.5M NaCl solution for 30 and 60 min. annealed samples	64
Figure 41: Combined Polarization curves in 0.1M NaCl+ 0.1M H ₂ SO ₄ solution for 30 and 60 min. annealed samples	66
Figure 42: Combined Polarization curves in 0.5M NaCl solution for 30 and 60 min. annealed samples	69
Figure 43: Combined Nyquist plot in 0.1M NaCl+ 0.1M H ₂ SO ₄ solution for 30 and 60 min. annealed samples	71

LIST OF ABBREVIATIONS

SSs	:	Stainless steels
PM	:	Powder Metallurgy
SEM	:	Scanning electron microscope
SCE	:	Saturated calomel electrode
PDP	:	Potentiodynamic polarization
LPR	:	Linear polarization resistance
EIS	:	Electrochemical impedance spectroscopy
ECAP	:	Equal Channel Angular Pressing
AES	:	Auger Electron Spectroscopy
E_{corr}	:	Corrosion potential
i_{corr}	:	Corrosion current density
E_{pit}	:	Pitting potential
i_{pass}	:	Passive current density
R_f	:	Film Resistance
R_{ct}	:	Charge transfer resistance
CPE_f	:	Constant phase elements of solution/film Interface
CPE_{dl}	:	Constant phase elements of solution/substrate Interface
R_p	:	Resistance polarization
R_s	:	Solution resistance

|

ABSTRACT

Full Name : [Nabeel Ameer]
Thesis Title : [Investigating the Electrochemical Properties Of a newly developed Fe-Cr Alloy (Fe-18Cr-XSi) With Silicon addition]
Major Field : [Material Science & Engineering]
Date of Degree : [December 2017]

Nowadays, Stainless steels (SSs) are used in different industries like Oil & Gas, Chemical-Pharmaceutical, Medical & Transport because of their excellent corrosion resistance. SSs is an alloy of iron mainly consisting of Fe, Cr and small amount of other alloying elements. SS attain their “stainless” character owing to an oxide film which provides remarkable resistance to corrosion. Alloying elements in the SSs helps in strengthening the passive film. Due to variety of demands in different industries, many types of SSs have been developed. SSs are classified into four main groups based on composition and processing techniques. i.e. Ferritic, Austenitic, Duplex, and Martensitic stainless steels. Many researchers have reported the beneficial effects of “Silicon” addition in Fe-Cr Alloy (Stainless Steel) and it is believed that, presence of “Silicon” improves localized corrosion resistance, passivation ability and pitting resistance.

In this research, Fe-18Cr-XSi (X=0-4) Ferritic Stainless Steels with silicon content varying from **0 - 4%** were prepared from vacuum arc melting followed by rolling and annealing at two different time durations. Different Electrochemical techniques were used to study the effect of silicon and grain size on the corrosion properties in the designed alloys.

Potentiodynamic polarization (PDP) results revealed that, by increasing the silicon content in **Fe-18Cr-XSi (X=0-4)** alloy, the electrochemical properties like corrosion potential (E_{corr}) and Pitting potential (E_{pit}) were improved significantly. Electrochemical Impedance spectroscopy (EIS) results showed higher values of resistance polarization (R_p) for samples with high amount of silicon. Such results are indicative of a stronger and more stable passive film. Electrochemical studies on samples with fine grain size revealed better electrochemical properties when compared with relatively coarser grain size samples.

ملخص الرسالة

الاسم الكامل: نبيل أمير

عنوان الرسالة: لتحقيق في الخصائص الكهروكيميائية من الحديد المطورة حديثاً سبائك الكروم (Fe-18Cr) مع إضافة السليكون

التخصص: ماجستير في علوم المواد والهندسة

تاريخ الدرجة العلمية: ديسمبر 2017

في هذه الأيام يستخدم الفولاذ المقاوم للصدأ في صناعات مختلفة مثل النفط والغاز والعلاجات الكيميائية والنقل وذلك بسبب كفاءته العالية لمقاومة التآكل. الفولاذ المقاوم للصدأ هو عبارة عن مجموعة عناصر تتكون أساساً من الكروم وخليط مختلف من العناصر الأخرى. وتعرف المعادن المقاومة للصدأ بتحقيق طابعها في خاصية عدم التآكل من خلال وجود الأكسدة التي توفر مقاومة ملحوظة للصدأ. ويعتبر وجود العناصر في المعادن المقاومة للصدأ يساعد في تعزيز الأكسدة. وبسبب وجود مجموعه متنوعة ومختلفة في متطلبات في مجال الصناعي وضعت أنواع كثيرة من الفولاذ المقاوم للصدأ. ويتم تصنيف الفولاذ المقاوم للصدأ إلى أربع مجموعات رئيسية بناءً على أسس التكوين والتقنيات المعالجة. فبريتك أوستنيتي دوبلكس ومارتنسيتيك وقد اكتسب في السنوات القليلة الماضية الفولاذ المعروف باسم العناصر الثلاثية شعبية كبيرة بسبب خصائصها الكهروكيميائية. وقد أفاد العديد من الباحثين عن فائدة أثار إضافة السليكون في سبائك الحديد والكروم ويعتقد أن وجود السليكون يحسن من مقاومة التآكل والقدرة على التحمل ومقاومة التآليب.

وفي هذا البحث تم تحطير (Fe-18Cr) بمحتوى السليكون يتراوح ما بين 0-4 % وقد تم استخدام تقنيات كهروكيميائية مختلفة لدراسة تأثير السليكون كما تم تحديد تأثير حجم الحبوب على الخصائص الكهروكيميائية عن طريق تغير حجم الحبوب في أوقات مختلفة.

وكشفت نتائج الأستقطاب بوتيني ديناميك (PDP) أنه من خلال زيادة محتوى السليكون في سبائك الحديد-الكروم، فإن الخصائص الكهروكيميائية مثل إمكانات التآكل (E_{corr}) وإمكانات التآليب (E_{pit}) تتحسن بشكل ملحوظ مما يؤكد القدرة على وقاية الأكسدة. وكشفت نتائج التحليل الكهروكيميائية مقاومة (EIS) أيضاً قيم أعلى من مقاومة الاستقطاب لعينة مع نسبة عالية من السليكون. النتائج هي أيضاً مؤشراً على قوة الأكسدة وأكثر استقراراً. وكشفت الدراسات الكهروكيميائية على أن العينات ذات الحجم الصغير من الحبوب تتميز بخصائص مقاومة للصدأ أفضل عند مقارنتها مع عينات ذات حبوب خشنة نسبياً.

CHAPTER 1

INTRODUCTION

1.1. Corrosion & Stainless Steels (SSs)

Almost everyone is familiar with corrosion in one form or the other i.e pipe leaks, rusting in the fence or light towers, rusting in bolts, etc. Structural metals are usually made from their ores; large amount of energy is applied to convert ores into some useful metallic product which puts them in a metastable state. Thermodynamically, everything in this world tries to go back to its stable state, so when metals come in contact with the atmosphere or corrosive media they react chemically and form oxides which are somewhat similar to their original state. Oxides have poor mechanical properties and are not useful. So by definition “Corrosion is the deterioration of materials by chemical interaction with their environment”.

In modern society, corrosion is a serious problem and the cost of corrosion is estimated to be hundreds of billions of dollars yearly. The consequences of corrosion are many due to which different catastrophic failures had occurred and huge amount of money had been lost along with the loss of human life. Major accidents due to corrosion are sinking of Erica, Bhopal accident, Mihama-3 incident, Silver bridge collapse and many more.

Metals are widely used in engineering applications and are prone to corrosion during service. Metals undergo corrosion when they come in contact with the environment. Every environment has different effect on the metals; some are corrosive in nature to some metals and some are not. So, it is very important to use only those materials which are corrosion resistant in their respective environments like Carbon steels in general

atmosphere, SSs in acidic and sea water environments etc. The best way to combat corrosion is to develop materials which are not only corrosion resistant but also provide better mechanical properties. Sometimes, materials only cannot help to attain corrosion resistance; that is why different protection strategies are developed to combat corrosion.

Some of the common protection strategies are

1. Coatings
2. Cathodic Protection
3. Inhibitors

Lately, Iron-Chromium alloys have become extremely useful and important in scientific and industrial fields. Due to their unique crystallographic, magnetic and corrosion properties, these alloys have been widely used in alloy development for testing various models and theories. The main importance of these alloys in industrial applications is due to their low ductile-to-brittle transition temperatures and high corrosion resistance. Due to these useful properties, Iron-Chromium alloys have been used in industry like steel-making as a basic ingredient.

The chemical and mechanical properties of the Iron-Chromium alloy are mainly influenced by the crystal structures. Pure iron usually exists at room temperature in the form of a Ferritic structure which is a body-centered cubic structure (bcc) also known as alpha phase (α). There are other structures as well which can form due to the change in temperature and have different properties and crystal structures. The alpha Ferrite can be transformed into face-centered cubic structure of Austenitic (fcc) Gamma phase (γ) when heated above 910°C. The Iron-Chromium phase diagram (Figure 1) shows the

composition and temperature regions where Ferrite, Austenite, Martensite and Sigma phase are stable. Chromium is considered to be the Ferrite stabilizing element and it helps in expanding α phase field. When the chromium content is increased ($>13.4\%$) in the Fe-Cr alloy the α phase will become stable Ferritic structure starting from solidification to room temperature

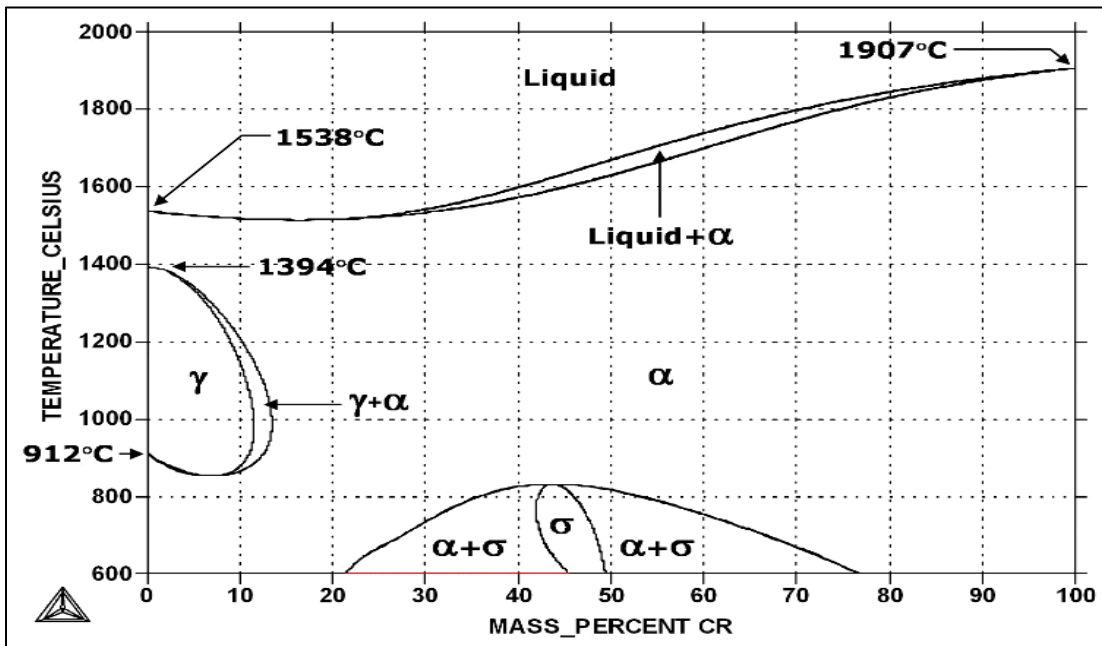


Figure 1: Binary iron-chromium equilibrium phase diagram [1]

SSs are one of the most important and popular materials which have excellent electrochemical properties and good strength. Although, the consumption of SSs were not that high when compared to that of carbon steels, still, SSs growth has been steady. Major applications of SSs include consumer products, plant and equipment for oil and gas, chemical process, beverage and food industries. The most widely used grades of SSs are Austenitic and Ferritic.

Most iron alloyed steels can be easily corroded in air or acid environments. However, SSs offer excellent corrosion resistance in different environments such as seawater, diluted and concentrated acids, and high temperature environments.

SSs attain their stainless character because of the chromium (Cr) content (minimum 10.5%). SSs are not inert unlike noble metals such as gold which has excellent corrosion resistance. Instead, the presence of Cr and due to its reactive nature, the surface layer of corrosion product becomes sufficiently adherent and impenetrable. This stops the reactivity of Cr by acting as a barrier between the base material and the environment. This resistance to corrosion is called passive behavior or “passivity”.

Corrosion resistance of SSs comes from a thin chromium oxide (Cr_2O_3) layer that develops on metal surface and imparts stainless quality to SSs. The passive film that develops on SSs surfaces is made up of oxides of iron (Fe) and Cr. In dry and clean conditions, chromium oxide passive film can easily form on surface of SSs with excellent protective ability (Figure 2). In order to understand and learn about the passive film growth and kinetics, various theories have been published.

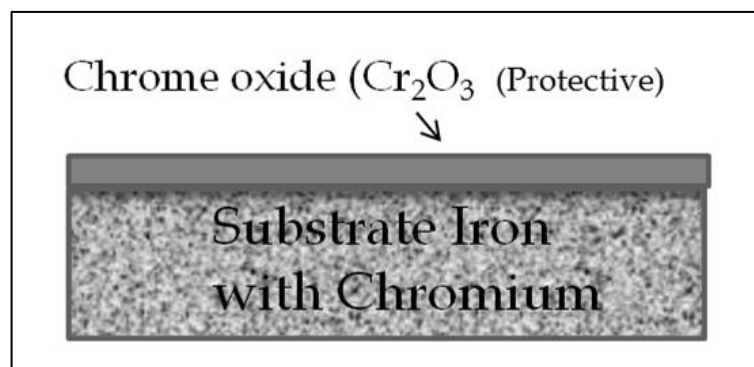


Figure 2: Schematics of the Chromium Oxide (Cr_2O_3) present on SSs

1.2. Passive Film on SSs

Michael Faraday gave the first theory of passive film formation in 19th century. The study was carried out on iron surfaces. The results revealed that the iron surface is 'altered'. Uhlig et al. [2] published a review which summarizes detailed research on passive films. Sato et al. [3] also published an introduction to passivity theory. High Field Models of Gunterscultze et al. [4], [5] and [6], Verwey et al. [7], Cabrera and Mott [8], and Fehlner and Mott [9] are some of the models that are suggested to model the behavior of passive layers. However, all these models have certain shortcomings, these models did not take into account the existence of steady-states in both the passive current density and the film thickness and also multi-layer passive films were not taken into consideration.

Because of these deficiencies the most comprehensive model of passive film was proposed by Macdonald [10] and co-workers. The model is known as "Point defect model" (PDM) (Figure3). This model incorporated the bi-layer structure of the passive film which comprised of a defective oxide barrier layer which formed adjacent to the metal and an outer layer that is formed by precipitation product. Precipitation product was developed due to the reaction of transmitted cations with species in the environment. This, model also introduced metal interstitials to the site of defects, recognized barrier layer dissolution, and the need to classify reactions as to whether they are lattice conservative or non-conservative. PDM-II has enjoyed considerable success in modeling the behavior of passive films and has been widely used by different researchers in their researches.

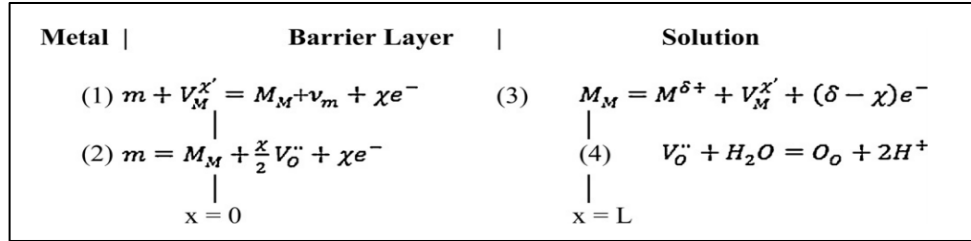


Figure 3: Point defect model for generation and annihilation of cation vacancies [10]

It is well known fact that Cr content in SSs is the main alloying addition that increased its resistance to corrosion; more the Cr content, more will be the corrosion resistance. Cr content is usually in the range of 10-30 % wt. in SSs. The reason of this increased corrosion resistance is because of the stable Chromium-oxide layer on the surface of the specimen. Presence of Cr in stainless steel causes the enlargement of a pH region of stable passivity. It also decreases the passive current density and shift repassivation potential to more negative potential. It has also been reported that, pitting resistance is also increased because of the presence of Cr. The passive film is formed because of the selective dissolution of Fe and formation of Cr oxides. The role of alloying elements in developing passive film had been studied widely and it was suggested that, Cr content should be more than 50% in the passive film to make it stable. The percentage of the Cr content in passive film increases with the increase in Cr content of the alloy.

However, in highly corrosive environments, only Cr is not sufficient to attain better corrosion resistance, instead, some other elements are required to increase the corrosion resistance. So, because of this reason many modern SSs contain specific alloying elements which enhance specific properties.

Passive films are susceptible to break down in aggressive solutions, pH changes and temperature. Breakdown of passive films lead to a phenomenon called “pitting”. Pitting can be characterized in three stages: [11]

- (1) Passive film breakdown and the nucleation of pits.
- (2) Metastable pitting in which the growth of the pits is halted which is approaching stability. Pits grow / develop for a specific time and for a specific size before repassivation. Pitting susceptibility can be proposed to be a measure of pitting.
- (3) Pit growth occurs until the interior of the pit is filled with electrolyte and repassivation is prohibited.

1.3. Types of SSs

Corrosion properties of the SSs can be increased by the addition of suitable alloying elements which have a direct influence on the passive film properties. Commonly used alloying elements are Nickel (Ni), Silicon (Si), Molybdenum (Mo) Carbon (C), Nitrogen (N), Titanium (Ti), Aluminum (Al), & Copper (Cu). These alloying elements impart different properties by affecting the microstructure of the materials. Based on microstructure and processing techniques SSs are divided into four major categories.

1. Ferritic SSs
2. Austenitic SSs
3. Martensitic SSs
4. Duplex SSs

1.4. Ferritic SSs

Ferritic SSs have a Ferritic crystalline structure, which is a body centered cubic crystal structure (BCC). In these types of SSs the structure remains Ferritic because these steels contain less Austenite forming elements, i.e. Nickel (Ni) and contains high amount of Ferrite stabilizer elements like Chromium (Cr).

Ferritic SSs grades are known to be the cost effective stainless steels as they do not contain Nickel as an alloy addition which is expensive. Cr percentage in Ferritic SSs varies from 10.5 - 29wt. % which makes this material corrosion resistant. These steels also contain some amounts of Molybdenum (Mo), Aluminum (Al) and Titanium (Ti). These steels have a higher mechanical strength than Austenitic SSs, but their ductility is less. They have ferromagnetic properties unlike Austenitic SSs which are not ferromagnetic. However; magnetism is not directly related to corrosion resistance. They cannot be hardened by heat treatment. The most widely used Ferritic SSs grades in the world are 409, 410 and 430. The applications in which these grades are used are washing-machine drums and exhaust systems. These materials are considered to have broader application potential, in numerous fields.

So, in this study a Fe-18Cr-XSi(X=0-4%wt.) Ferritic SS was designed and developed by only varying the percentage of silicon (Si) in order to investigate its independent effect on electrochemical properties. Effect of grains size by varying the solution annealing temperature was also investigated. |

CHAPTER 2

LITERATURE REVIEW

2.1. Role of Alloying Elements and Their Characteristics

SSs contain various distinctive alloying components, each of which specifically affects the properties of the steel. The properties of a particular steel grade will accordingly be determined by the amount of alloying elements in that specific grade.

A brief review of the alloying components and their effects on the properties and structure of the steel is given below with an explanation that why different elements are added to certain grades [12]

2.1.1. Chromium (Cr)

This is the most essential alloying element as it provides basic corrosion resistance to SSs. Generally better corrosion resistance is due to the higher content of Cr. At high temperature Cr also upgrades the steel's resistance to oxidation and promotes a Ferritic structure.

2.1.2. Nickel (Ni)

Ni promotes an Austenitic structure. It generally increases toughness and ductility. Ni also provides good effect in an acid environment and lowers the corrosion rate. Ni is used to form intermetallic compounds in precipitation-hardening steels to increase the strength of the steel.

2.1.3. Molybdenum (Mo)

Mo significantly increases the mechanical strength of steels and enhances the resistance to both localized and general corrosion. It also promotes a Ferritic structure and formation of secondary phases in Duplex, Ferritic and Austenitic SSs. At higher temperature, Mo increases the hardness in Martensitic SSs due to its effect on carbide precipitation

2.1.4. Manganese (Mn)

Mn is used to improve hot ductility in stainless steels. Ferrite / Austenite balance that varies with temperature is affected by the Mn, at high temperatures Mn is a Ferrite stabilizer and at low temperatures, it will stabilize Austenite. It is used to obtain high Nitrogen (N) contents in Austenitic steel and increases the solubility of N.

2.1.5 Copper (Cu)

This element generally promotes Austenitic structure and enhances the corrosion resistance of steels in some acid environments. Cu is used to increase the strength of steel by forming the intermetallic compounds in precipitation-hardening steels.

2.1.6. Nitrogen (N)

N promotes an austenitic structure because it is a very strong Austenite former. When N is used in combination with Mo then it enhances the resistance to localized corrosion. It is also used to increase the mechanical strength of steel. N will lead to a significant reduction in corrosion and toughness resistance in Ferritic stainless steels. In Martensitic-Austenitic and Martensitic SSs, the addition of N will reduce the toughness of the steel and gradually increases the hardness and strength.

2.1.7. Carbon (C)

C is a strong Austenite former and promotes an Austenitic structure. It also helps in achieving better mechanical strength. Higher C content affects resistance to intergranular corrosion. Higher C content also reduces both corrosion resistance and toughness in Ferritic SSs whereas in the Martensitic and Martensitic-Austenitic steels, it increases the strength and hardness. In Martensitic steels, strength and hardness is generally increased by reducing the toughness.

2.1.8. Titanium (Ti)

This element is a strong carbide and ferrite former and helps to promote a Ferritic structure and lower the effective carbon content. Ti is added in Austenitic steels to improve the resistance to intergranular corrosion, but at high temperature, it also enhances the mechanical properties of the steel. In Martensitic steels, Ti is used to increase the tempering resistance and reduces the Martensite hardness. By lowering the amount of interstitials in solid solution, Ti is added in Ferritic stainless steels to improve toughness and corrosion resistance.

2.2. Alloy development using Schaeffler Diagram

In order to understand the composition of the SS / alloy development, a Schaeffler diagram [13] can be used. This diagram (Figure 4) represents the effect of the proportion of two elements on the micro structure obtained after rapid cooling from 1050°C to room temperature. The X-axis of the diagram shows chromium equivalent (Cr_{eq}) which is calculated by adding the percentages of Cr, Mo, Si and Nb. All these elements are Ferrite stabilizers and higher Cr_{eq} number enhances the chances of the alloy to be in

stable Ferritic phase range. The Y-axis of the diagram shows Ni equivalent (Ni_{eq}) which can also be calculated by the addition of the percentages of Ni, Mn, N and Cu. These elements are Austenite stabilizers and higher Ni_{eq} number will shift the alloy into stable Austenite phase range. Calculation can be carried out by using following equations

$$Ni_{eq} = \%Ni + 0.5\%Mn + 20 \cdot \%N + 0.25 \cdot \%Cu$$

$$Cr_{eq} = \%Cr + \%Mo + 1.5\%Si + 0.7 \%Nb$$

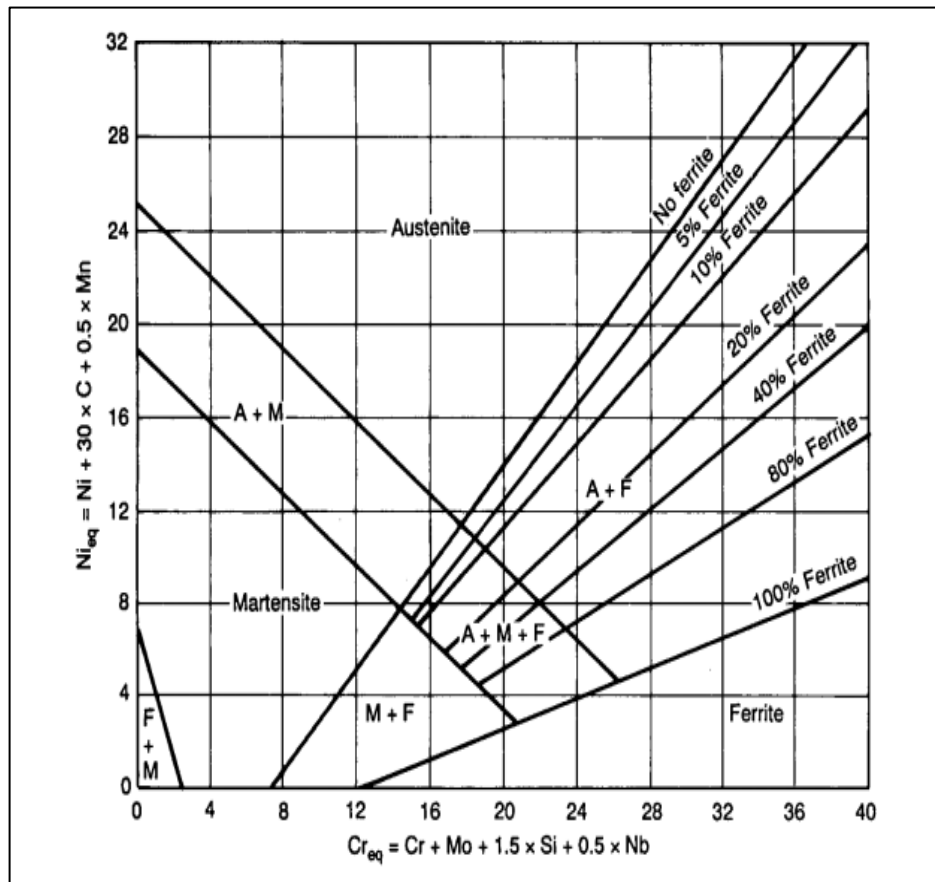


Figure 4: Schaeffler diagram showing phases present in as- solidified stainless steels at room temperature [13]

Based on Ni and Cr equivalents, the diagram shows four different compositional areas which depict the presence of different phases of SSs like Austenite, Ferrite, Martensite

(and mixtures of two or three phases). By using this diagram and calculating Ni & Cr-equivalent the content of Martensite, Austenite and Ferrite can easily be predicted in the resulting microstructure of the alloy.

2.3. Role of Silicon(Si) Addition on the Corrosion Properties of Steels

Si is found in different types of steels which is added intentionally or it is available in residual form such as ore or as a deoxidizing agent. In steel making, Si is used to remove oxygen from the molten melt which is considered to be a very good deoxidizing agent. In steel making, different types of additives are available which contain Si, among which the most common are silico manganese (Si-Mn) and ferrosilicon (Fe-Si). Si concentration in steels depends on the type of steel. In Semi killed steels, Si is found up to 0.10 % max. In Fully killed steels Si concentration reached up to 0.60 % max. Si imparts hardening effect to Ferritic phase in steels and because of this reason Si killed steels are harder and stiffer as compared to Al killed steels. Si also helps in increasing hardness and strength of the steel. Acid resistance can also be enhanced by the addition of small quantities of Si in steels. Magnetic permeability of the steels increases as Si helps in achieving coarser grain sizes. Dissolution of Si in iron strengthen it's structure. Si up to 0.50-1.0 % wt. is usually added in weld metal as a deoxidizer. Filler metals containing Si are used for welding and the weld metal strength is increased, however, as the strength is increased the ductility also decreases which intensify cracking problems in the weld.

Si is added in the SSs in small amounts. Main benefit Si provides is the attraction of oxygen towards itself during steel making. Different studies have shown the beneficial effect of Si at high temperatures in both Austenitic [15-17] and Ferritic SSs [18-20] due to the reduction of oxidation rate. Researchers explain this decreased oxidation rate is due

to the establishment of SiO_2 layer in between the base metal and the Cr layer. This layer act as a barrier to diffusion and to transport of cation from the base metal [17, 19]

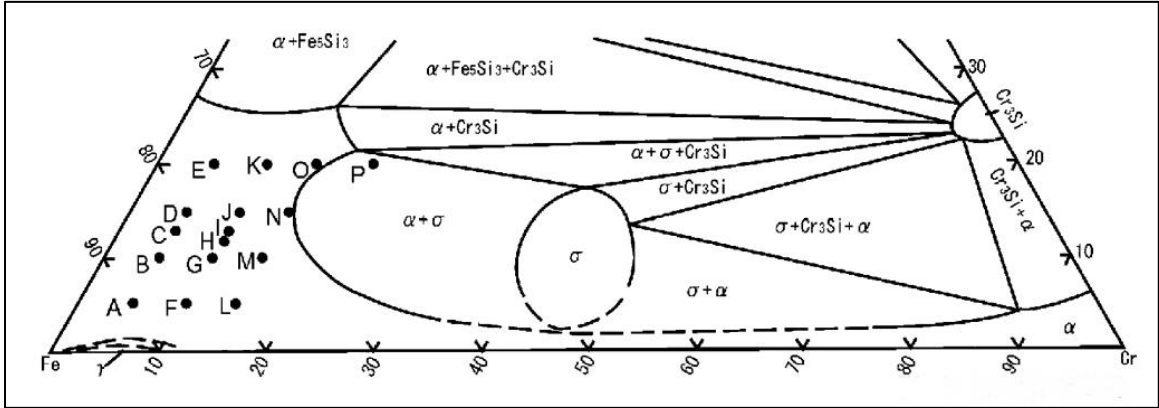


Figure 5: Phase diagrams of Fe-Cr-Si ternary iron alloy [14]

I. Svedun et al. [21] investigated the influence of Si on the oxidation resistance of SSs by varying the composition of Si from 0.06 to 5.3%. Samples were oxidized at different temperatures. The oxide films were investigated with an X-ray diffractometer and SEM with an electron probe.

As shown in Figure 6 & 7, the lowest weight gain was observed at 800 °C and 1000 °C for sample containing 5.3% Si (Sample No. Si5). This means that oxidation rate is very low and the oxide layer is protective which resists further oxidation at high temperatures.

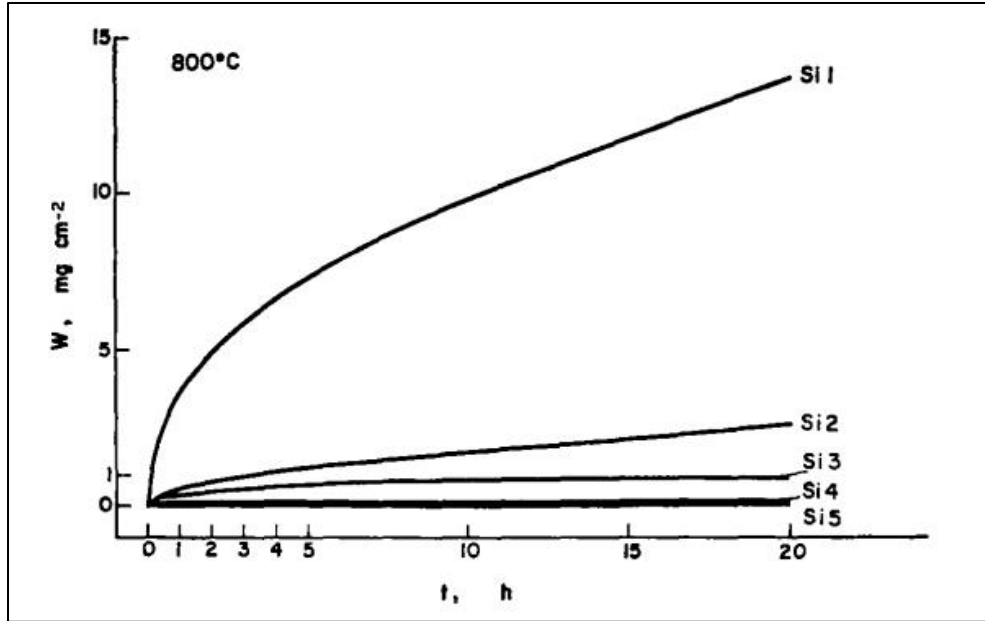


Figure 6: Variation in weight with respect to time for samples Si1-Si5 with different silicon contents during isothermal oxidation at 800 °C [21]

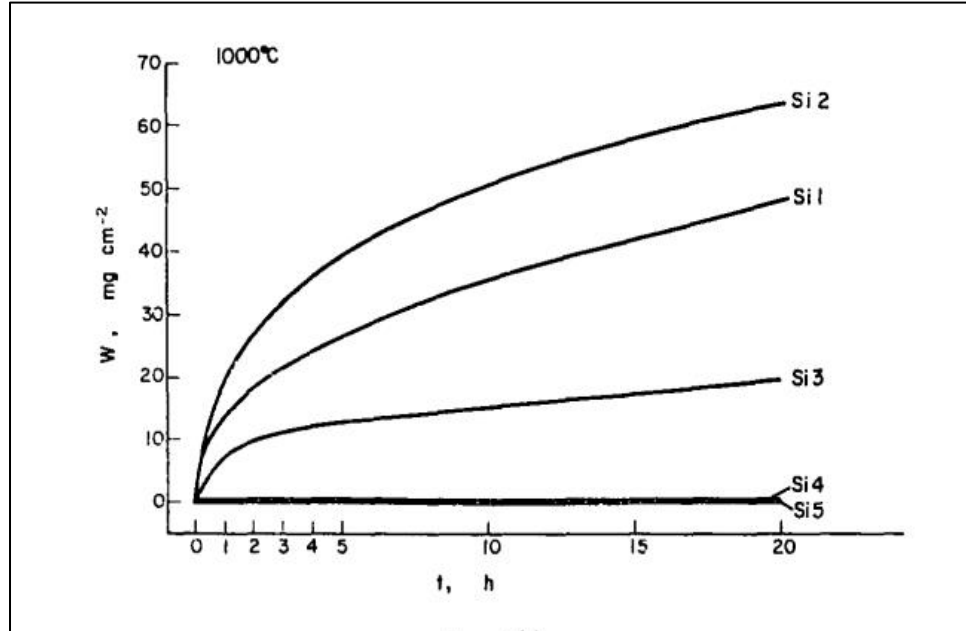


Figure 7: Variation in weight with respect to time for samples Si1-Si5 with different silicon contents during isothermal oxidation at 1000 °C [21]

The reason for the improved oxidation resistance is because of the low diffusion rate of Fe through a SiO₂ film. This low diffusivity reduced the oxidation rate of an Iron-Silicon (Fe-Si) alloy appreciably.

Si also improves the localized corrosion resistance of SSs. Several researchers have done investigations by using Austenitic and Ferritic SSs, both in sintered and wrought conditions, to determine the effect of Si on localized corrosion resistance. The beneficial effect of Si addition in sintered SSs has been observed. Si promotes liquid phase sintering due to which the more dense structure is obtained in the sintered SSs with less porosity, hence corrosion resistance is enhanced [20, 22, 23].

Wen-Ta Tsai et al. [22] used Austenitic SSs which were developed by using powder metallurgy (PM) technique to study the influence of Si on corrosion resistance. To determine corrosion resistance of the sintered SSs, Potentiodynamic polarization (PDP), corrosion rate and corroded surfaces were studied to determine the corrosion resistance. Samples were prepared by using 304L SS powder with composition 18.9Cr -10.9Ni. Si content varied from 0-5 % wt. Samples were tested in 3.5M NaCl solution and 6wt% ferric chloride FeCl₃ solution.

It was found that by adding Si, density of SSs was increased and the reason was the formation of liquid phase between Si and SS powder. Improved sintering rate and better densification was achieved by the formation of the liquid phase.

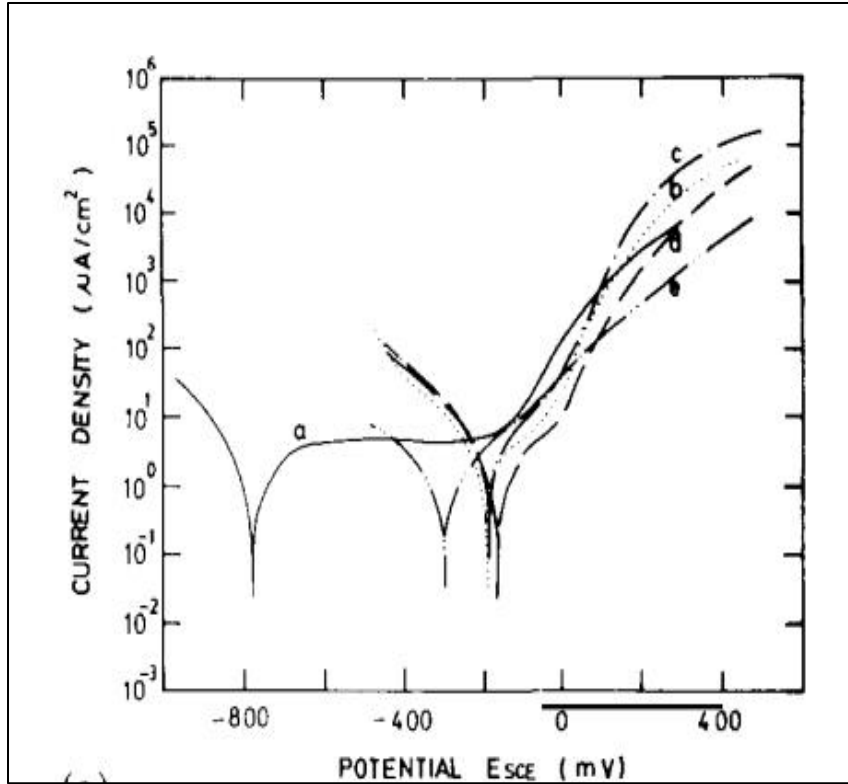


Figure 8: Potentiodynamic polarization spectra for sintered SSs in 3.5 wt.% NaCl solution a, IM 304L SS; b, PM 304L SS; c, PM 304L SS + 1 wt.% Si; d, PM 304L SS + 3wt% Si [22]

In Figures 8 & 9, PDP curves show that PM alloy (PM 304L SS + 3wt% Si) achieved passivity and sample with 3 wt.% Si had achieved more negative corrosion potential in both the NaCl and FeCl₃. However, because of the aggressive nature of the solution of Ferric chloride no passive behavior was observed. Corrosion calculation also suggests that samples with high Si content have more corrosion resistance.

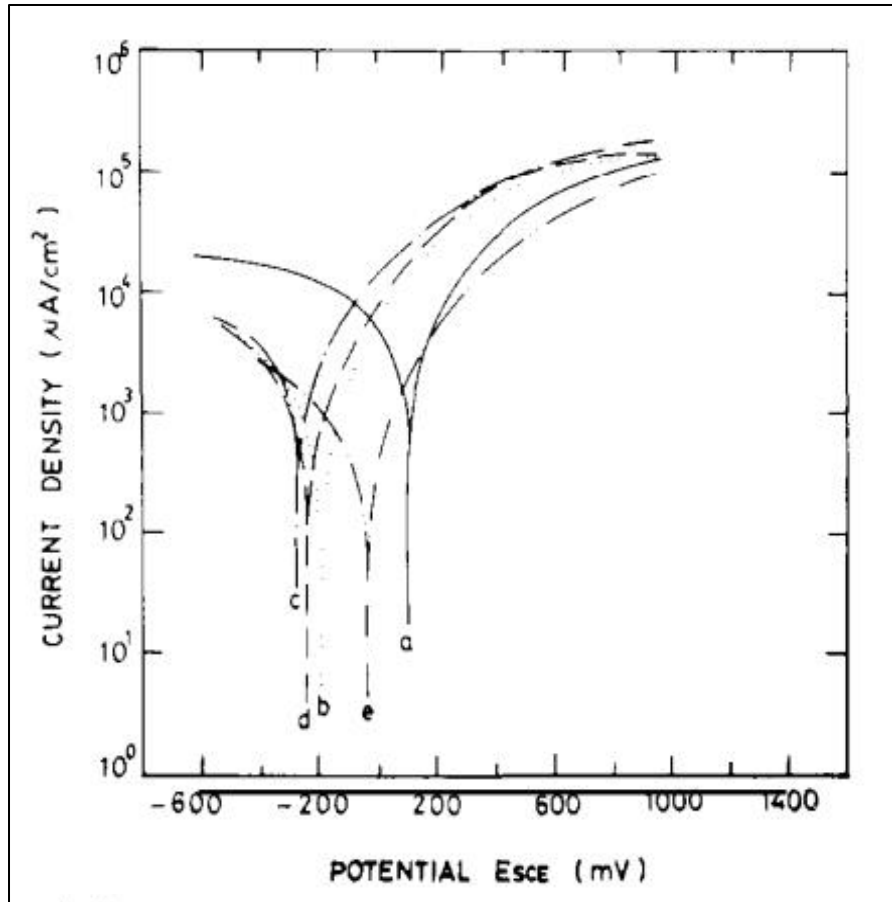


Figure 9: Potentiodynamic polarization spectra for sintered stainless steels in 6 wt.% FeCl₃ solution (pH 1.6) at 25 °C: a, IM 304L SS; b, PM 304L SS; c, PM 304L SS + 1 wt.% Si; d, PM 304L SS + 3wt% Si[22]

F. Velasco et al. [23] also published research on SSs developed via PM technique. SSs were manufactured from pre alloyed powders of 434L and 2% Si was added to check the effect on corrosion properties. Comparison was done with the same samples prepared by using the same composition but with less Si content. In order to determine the electrochemical properties PDP experiments were conducted in 0.1 Molar Na₂SO₄ solution at ambient temperature.

PDP experiments (Figure 10) revealed that sample 434L + 2% Si shows lower corrosion current (i_{corr}) than 434L steels without Si. SSs with more Si show more stable passive

behavior. Favorable effect of Si was confirmed by the higher E_{CORR} which was better than SS 434L.

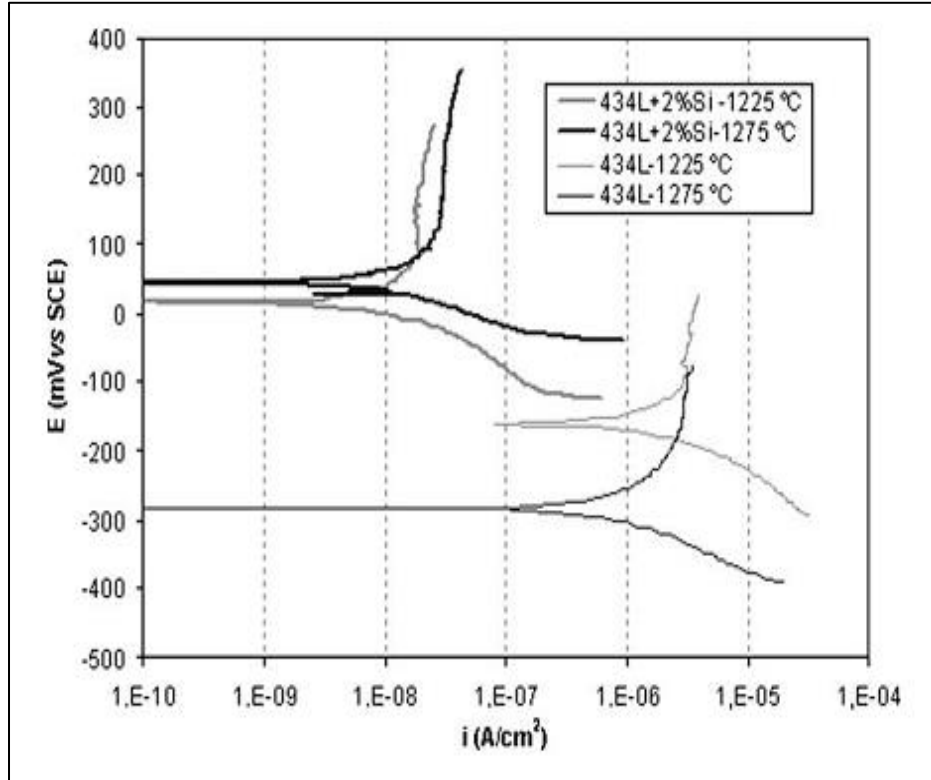


Figure 10: Polarization spectra of Powder Metallurgy SS after oxidation [23]

The beneficial effect of Si was described by the existence of Si in the passive layer which modifies the protective ability. Outer zone of the passivation layer contains localized Si rich layer and the protective ability of the SSs comes from the presence of Cr and Si.

Studies have also been carried out on wrought SSs containing Si, to detect the effect of Si on the corrosion properties. Corrosion studies of wrought SSs by Ion implantation and deposition have also been done at ambient temperatures in which Si ions are implanted / deposited on the surface of SSs. Si ions in the implanted layer inhibit the pitting

corrosion of the steels by the formation of SiO_2 which are placed in a very aggressive aqueous media [24-26]

Further studies of the effect of Si concentration on the corrosion resistance of SSs have been done by few researchers. T.N. Rhodin [27] found the positive effect of Si due to the increased stability of the passive state, which results in the increased Si content of the protective film.

Thomasov et al. [28] studied the effect of various alloying elements in SSs on pitting corrosion resistance. 18Cr-14Ni SSs samples with 5 wt% Si / V were tested in 0.1Normal NaCl solution. Addition of 5% wt. Si increases the breakdown potential. It was concluded that steel containing about 2.5 and 5 wt.% Si are the most resistant to pitting corrosion i.e higher pitting potential.

Blajiev et al. [29] investigated the influence of Si on the corrosion resistance of Fe-25Cr SSs with 1-5% of Si in 1Normal H_2SO_4 . It was observed that polarization curves of SS with Si containing 1 & 3 % are not that much different than the Fe-25Cr however, SSs with 5% Si shows more negative passivation potential and lower critical current potential (i_c). Polarization experiments shown in Figure 11 revealed that, sample Fe-25Cr-5Si (\square) has better electrochemical properties. After reviewing the PDP spectra it was observed that an addition of 5% of Si in the sample quickens the anodic dissolution and helps in reducing the cathodic reaction rate, and supports transition to passive state.

Mosebuer spectroscopy experiments were also carried out on Fe-25Cr and Fe-25Cr-5Si alloys. It was observed that Fe-25Cr-5Si has a more positive isomer shift compared to that of Fe-25Cr. Transfer of the electronic charge density is considered to be from Fe and Cr atoms to silicon. Strong interaction between Fe and Cr was also observed

because of depletion of the electronic charge density and, therefore, quickens the active dissolution of Fe-25Cr-5Si.

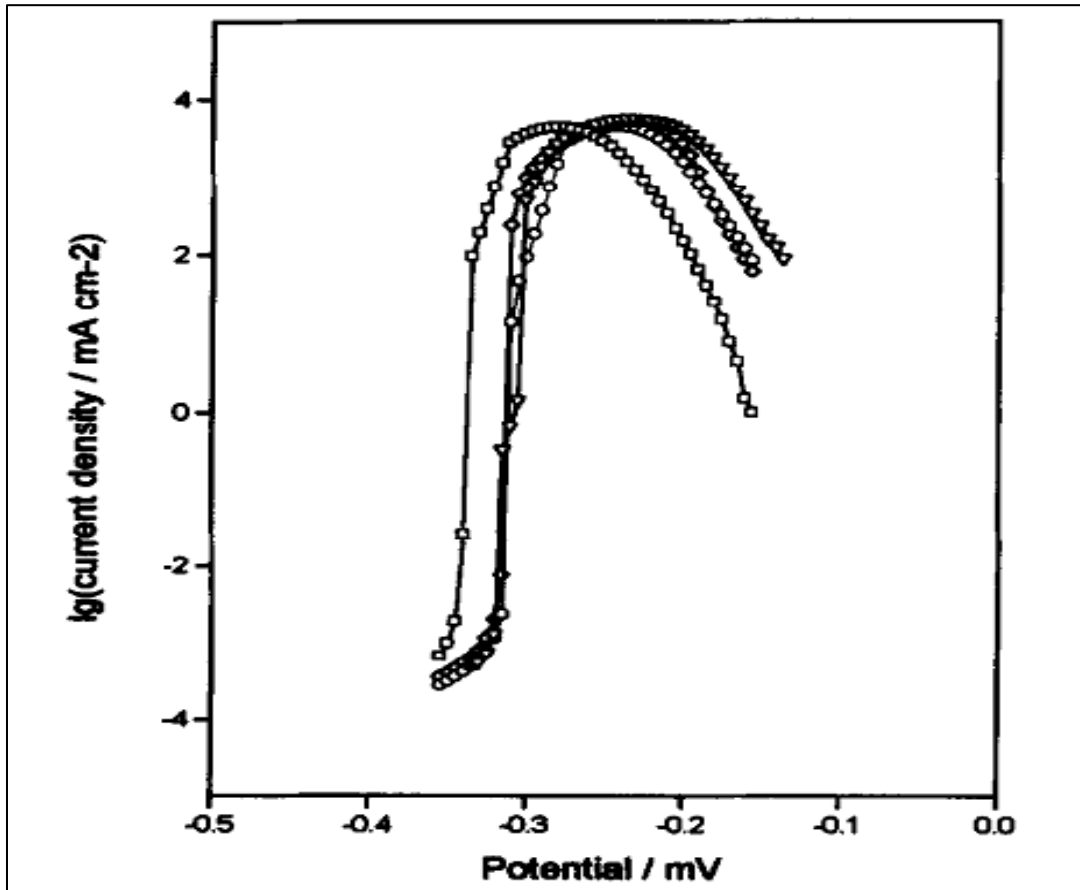


Figure 11: Potentiodynamic spectra obtained in 0.5 M H₂SO₄ at 25°C. Fe₂₅Cr (0); Fe₂₅Cr₁Si (0); Fe₂₅Cr₃Si (▼); Fe₂₅Cr₅Si (□) [29]

I. I. Reformatskaya et al. [30] also studied the effect of silicon on electrochemical properties. SS with composition Fe-8-13%Cr was selected and the Si content varied from 0.32-2.7%. By achieving this composition, limit of 14-15 atomic % of Cr and Si summary concentration was achieved. It was found that the critical summary concentration is because of the Si that builds up in the crystal lattice and its substitution of Cr atom. The pitting resistance was also studied in nearly neutral (pH 7.3–7.4) deaerated buffer solution containing 0.2 g/l NaCl. It was observed the values of pitting

potential E_{pit} achieved jump wise rise when the $C_{\text{Si}}+C_{\text{Cr}}$ concentration reached 14-15 at% and the E_{corr} values moves towards negative potential.

Katsuya Hoi et al. [31] also investigated the effect of silicon along with Mo and Al. Fe-10Cr composition was selected and composition of the alloy varied by adding Mo, Si and Al. Experiments were carried out in 0.5M H_2SO_4 and HCl solution. Potential Decay curves were used to study the stability of the passive films developed on the surface of alloys. Surface film studies by XPS/ AES were done to determine the passive film composition. Anodic polarization curves (Figure 12) revealed that Mo decreases the critical current density of Fe-10Cr-3Si alloy; however the current density increases in the transpassive region with the addition of Mo and Si. The Pitting potential of the alloys was also determined in 0.5 M NaCl solution and it was noted that Si and Mo enhances the pitting potential by moving the pitting potential in the more noble direction.

Chemical composition of the passive films was also analyzed using Auger Electron Spectroscopy (AES). Sample with composition Fe-18Cr-5Si was selected for analysis. It was observed in Figure 13 that passive film of sample containing Si shows the presence of Si which is concentrated on the surface layer along with Cr which is present in the shallow interior region. Fe and O was also detected which confirms the presence of iron oxide in the passive film. Figure 14 shows the schematic illustration of the enrichment of Cr and Si in the passive layer

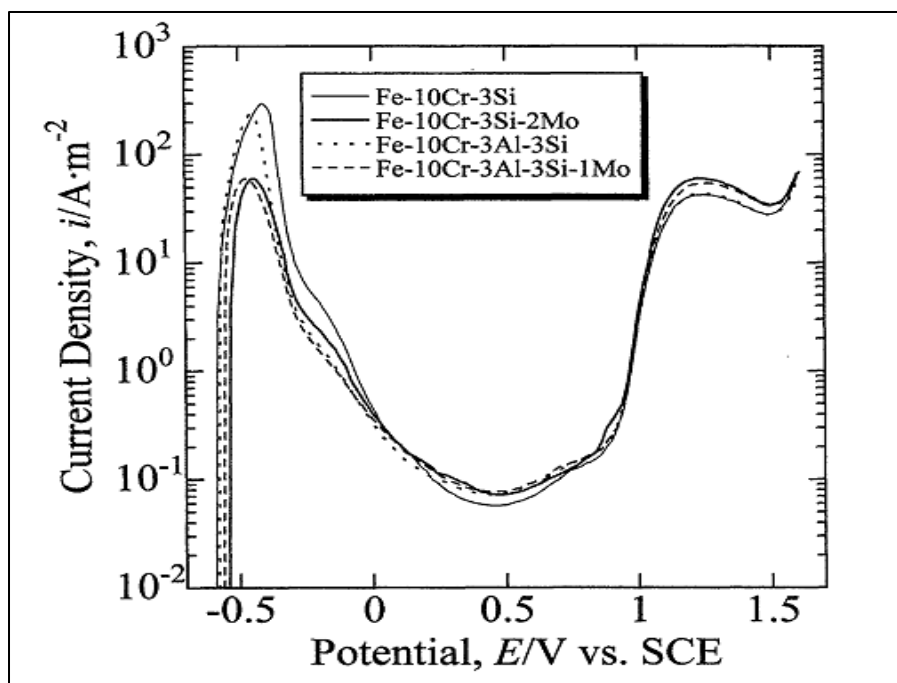


Figure 12: Effect of Al and Mo on polarization spectra of Fe-10Cr-3Si 0.5M H₂SO₄ solution [31]

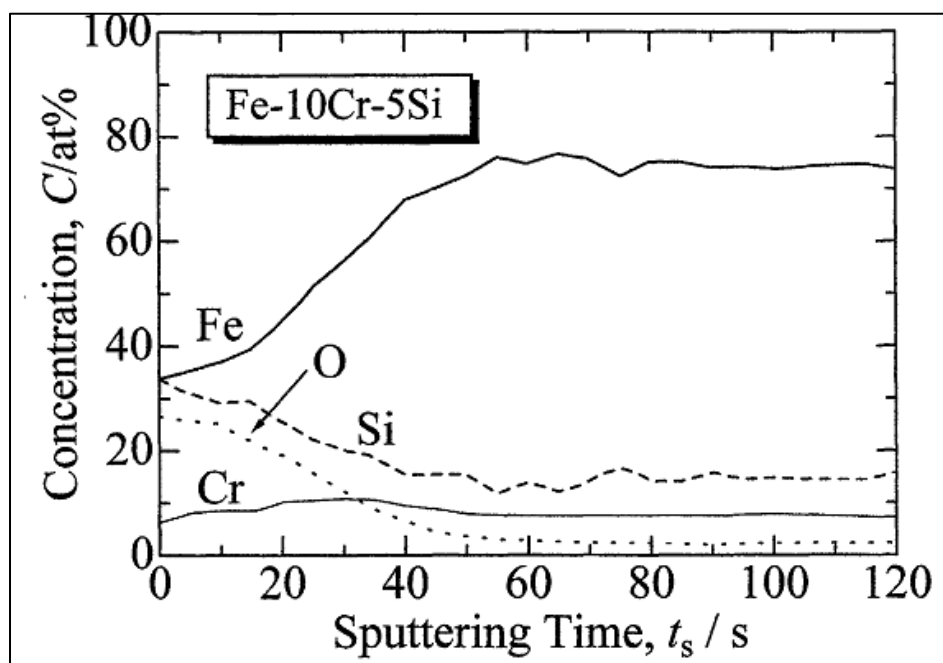


Figure 13: AES Depth profile of passive films developed on Fe-10Cr-5Si by passivation in 30mass% HNO₃ solution for 3.6ks [31]

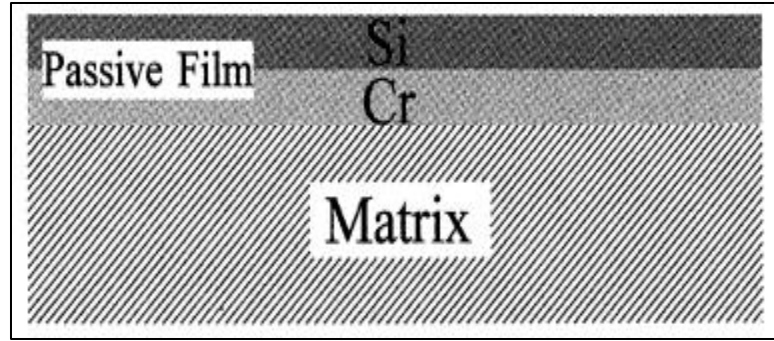


Figure 14: Schematic illustration of enrichment of Cr & Si in the passive film of Fe-10Cr-Si [31]

2.4. Advanced Electrochemical Techniques for Corrosion Testing of SSs

Studies on the passive film formed on SSs surfaces are of great importance. The studies and literature helped in understanding the electrochemistry of corrosion. In aggressive environments, collapse of passive films helps the dissolution at localized areas, which is considered to be main cause of corrosion failure. The composition of the alloy and environment are the two important factors on which the passive film properties depend. The reason is the change in thickness and composition in the film when it comes in contact with solution and different kind of charge transfers occur.

In recent years the Electrochemical Impedance Spectroscopy (EIS) becomes very popular to study the electrochemical systems. In its early days, EIS was used as a tool to investigate double layer capacitance but nowadays, this technique has been successfully used to determine the characterization of electrode processes and complex interfaces.

Electrochemical impedance is usually measured by applying an AC potential of an electrochemical cell and then measuring the current through the cell. The information about the interface, its structure and the reactions which are taking place at the interface can be obtained by using EIS technique.

EIS data helps in establishing an equivalent electrical circuit model for the electrochemical processes that are occurring at the electrodes. Equivalent circuit contains various elements that are related to the metal-film and film-solution interfaces and the phenomena occurring inside the passive film [32, 33]. It is because of EIS measurements, it is now possible to obtain information on the mechanism and development of the passive film growth model [34, 35].

Mansfeld et al. [37-39] has revealed that the changes in the impedance spectra can be used to detect the pitting corrosion of aluminum alloys. An estimate of pit growth rate has been made by Mansfeld et al. [39, 40]. The research of Scully et al. [41] indicates that, pitting resistance and passivity behavior of aluminum can be determined from impedance spectroscopy. EIS technique was also used to identify and observe pitting corrosion of materials other than Aluminum [42]. Oltra and Keddam [43, 44] compared theoretical model of pitting corrosion and impedance spectra. Different researchers studied the passive film formed on SSs by using EIS technique.

Cong-Cheng et al. [45] used EIS technique to find the effect of Cr on laser treated Fe-Cr and Fe-Cr-Si-N alloys in 3.5 wt.% NaCl solution. A simple Randles circuit was used as an equivalent circuit to fit curves. Nyquist plot (Figure 15) and resistance polarization values obtained from the curve fitting revealed that, sample with Fe-26Cr has the best passive film resistance.

EIS technique was also applied to determine the influence of Mo on the pitting resistance of 304L and 316L SS. The solution used was 5% NaCl solution at room temperature [46]. To model the behavior of alloy solution system, an equivalent circuit was developed.

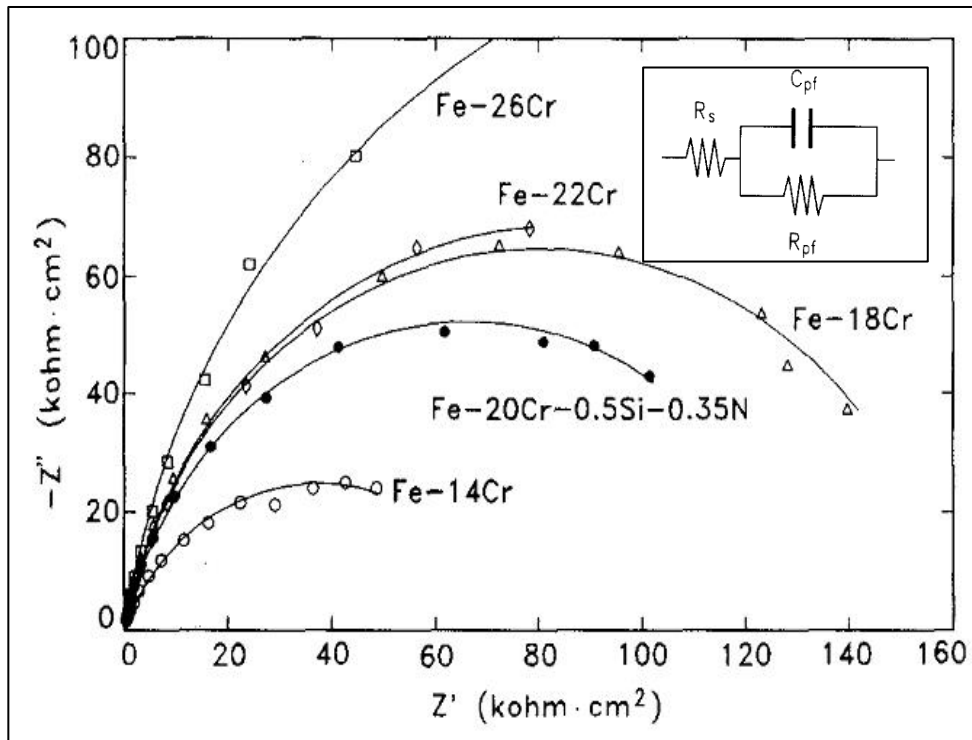


Figure 15: Nyquist plot of the laser treated samples with equivalent circuit [45]

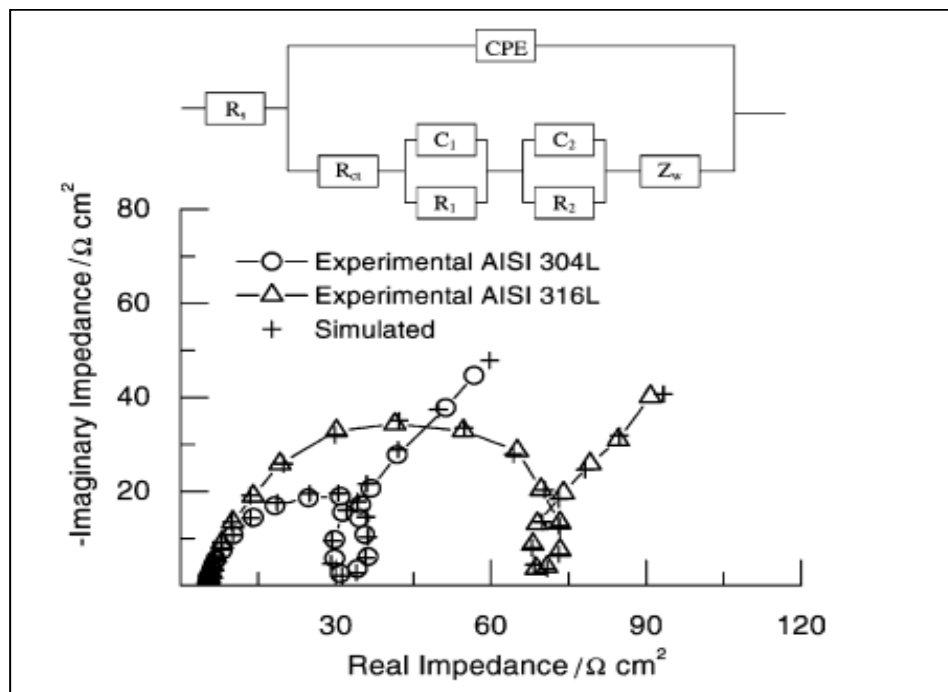


Figure 16: Nyquist plots for 304L (O) and 316L (▲) Stainless steel in 5% NaCl [46]

Nyquist plots (Figure 16) revealed capacitive behavior in the alloys. At higher frequencies, a depressed semicircle was observed which was due to the charge transfer

process. At intermediate frequencies, second capacitive loop was observed which is credited to adsorption desorption processes. At low frequencies a third capacitive response was observed which is linked to diffusion process happening in the pits through the corrosion products.

Electrochemical impedance spectroscopy (EIS) studies were also carried out on SSs which were coated. C.H. Lin et al. [47] used AISI420 stainless and mild steels which were coated with Cr-Al-Si-N layer. Studies were done in 3.5 wt.% NaCl solution and it was observed in Figure 17 that the coated SS420 sample with 11.5 at.% Si showed bigger capacitive loop as compared to mild steel coated sample (Figure 18). There is a significant improvements observed on charge-transfer resistance (R_{ct}) of coated SSs which contain high Si, however the coated mild steel shows no such trend and R_{ct} values were found to be on the lower side.

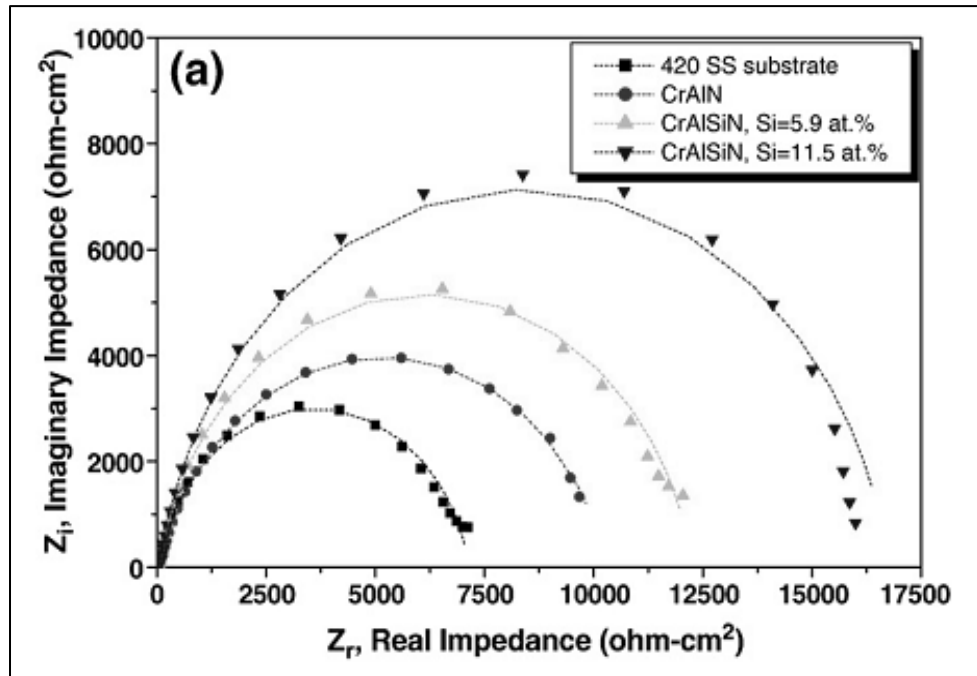


Figure 17: Nyquist plots of CrAlSi_xN/AISI420 [47]

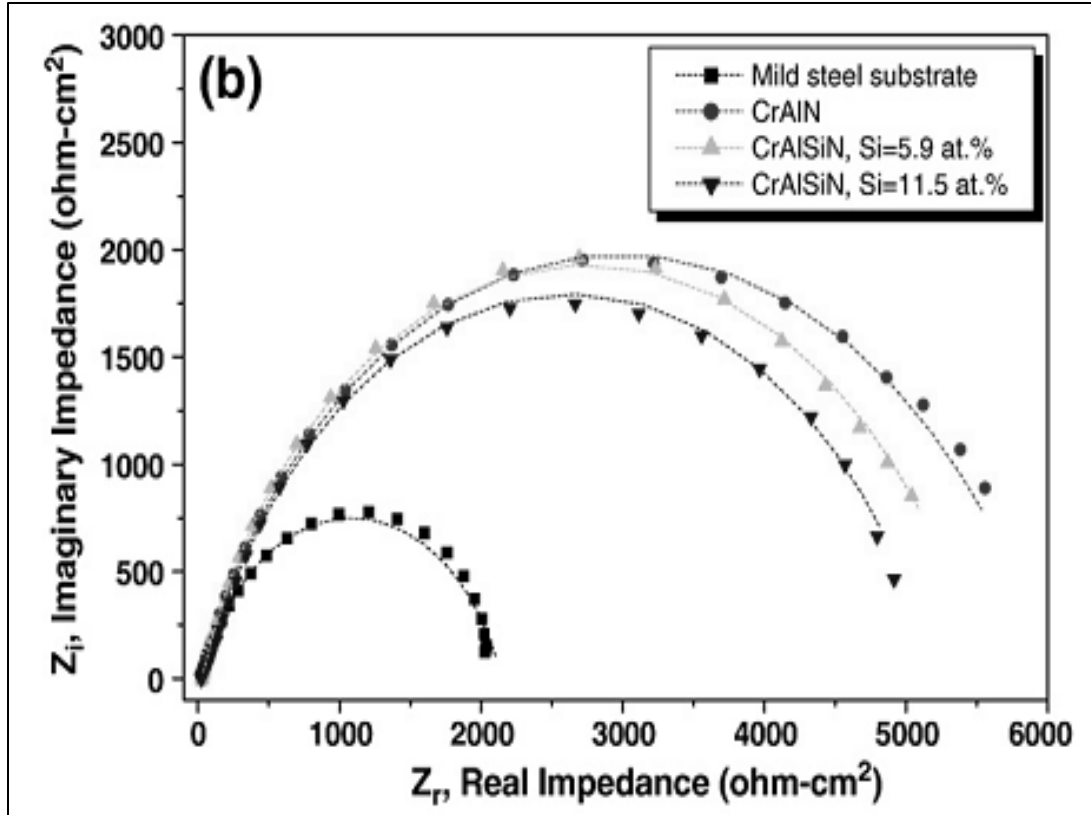


Figure 18: Nyquist plots of CrAlSi_xN/MS [47]

2.5. Effect of Grains Size on Electrochemical Properties

Grain size plays an important role in deciding the strength of the material as explained by Hall-Petch relationship that yield strength is inversely proportional to grain size [48, 49]. Varying the grain size of SSs has an appreciable effect on strength and toughness of the material [50, 51]. It is stated in literature, that the grain size not only affect strength of the materials but also affect corrosion resistance of the alloys especially in SSs. As compared to bulk material, the properties of grain boundaries are distinct in terms of atomic coordination and diffusion rates. Usually it is expected that high grain boundary densities (finer grains) surfaces show different electrochemical behavior than lower grain boundary densities surface (coarser grains).

A lot of work had been done by different researchers in order to find the effect of grain size on varieties of materials and by processing the material by different routes like rolling operations and severe plastic deformation (SPD) techniques and equal channel angular pressing (ECAP) [52-55]. After going through the scientific literature, beneficial effect of finer grains on the corrosion properties of stainless steels were found [56-59]. It has been reported that, by decreasing the grain size (grain refinement) electrochemical properties were greatly improved. [60-62].

Schino et al. [59] selected high Nitrogen Austenitic SSs and applied cold rolling and subsequent annealing (700 °C to 1000 °C) to obtain ultrafine grained samples in which the grain size varied from 2.4 μm to 25 μm . Microstructure of the alloy is shown in Figure 19.

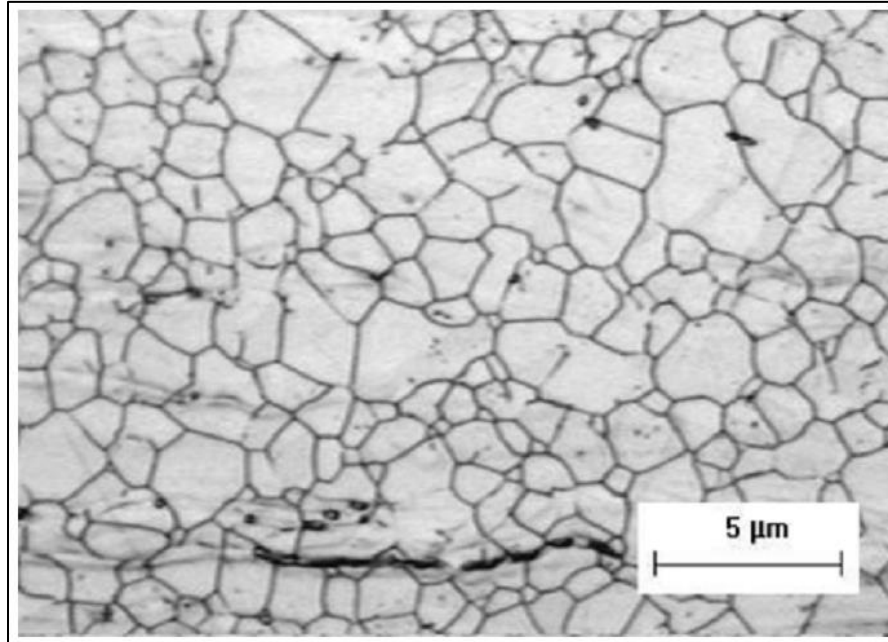


Figure 19: Microstructure of HN steel annealed at 900°C for 600s [59]

Pitting corrosion rate (PC) rate was also measured in a 10% FeCl₃-6H₂O solution at room temperature for 36 ks. The results obtained were then compared with AISI 304 steel. It was observed during Optical microscopy (OM) that, coarse grained steel samples provide limited sites for pitting to initiate. Pits observed were large and deep. In contrast, in fine grained steel, small pits were formed at several sites this phenomenon leads to a decrease of anodic current density as compared to coarse grains steel.

Hua Bing et al. [61] used polarization method on Ferritic SSs (15wt.% Cr) to find the effect of grain size on pitting corrosion resistance. Annealing was done at 1100 °C with annealing times varying from 0-60 minutes. By increasing the annealing time and cold reduction, different grain size samples were obtained in which the relatively coarser grain size was observed in sample with 60 min annealing as shown in Figure 20. Anodic polarization studies were carried out in 3.5wt % NaCl solution and the spectra obtained after test is shown in Figure 21. In samples with longer annealing time and coarser grains, the corrosion current density values were high and a smaller passive region was observed. Pitting corrosion resistance was also found to be decreased. In samples with finer grains size, this effect was absent as the pitting potential and passive range increased along with decrease corrosion current density. Cl⁻ adsorption in fine grain size steel decreased significantly which prevents the Cl⁻ diffusion in the passive layer as the passive film obtained was more compact.

Z.J Zheng et.al [62] studied the influence of changes in microstructure on the corrosion behavior of (ECAPed) 304 stainless steel samples. Nanostructure with grain size 80–120 nm was obtained after 4 and 8 passes ECAP as shown in Figure 22.

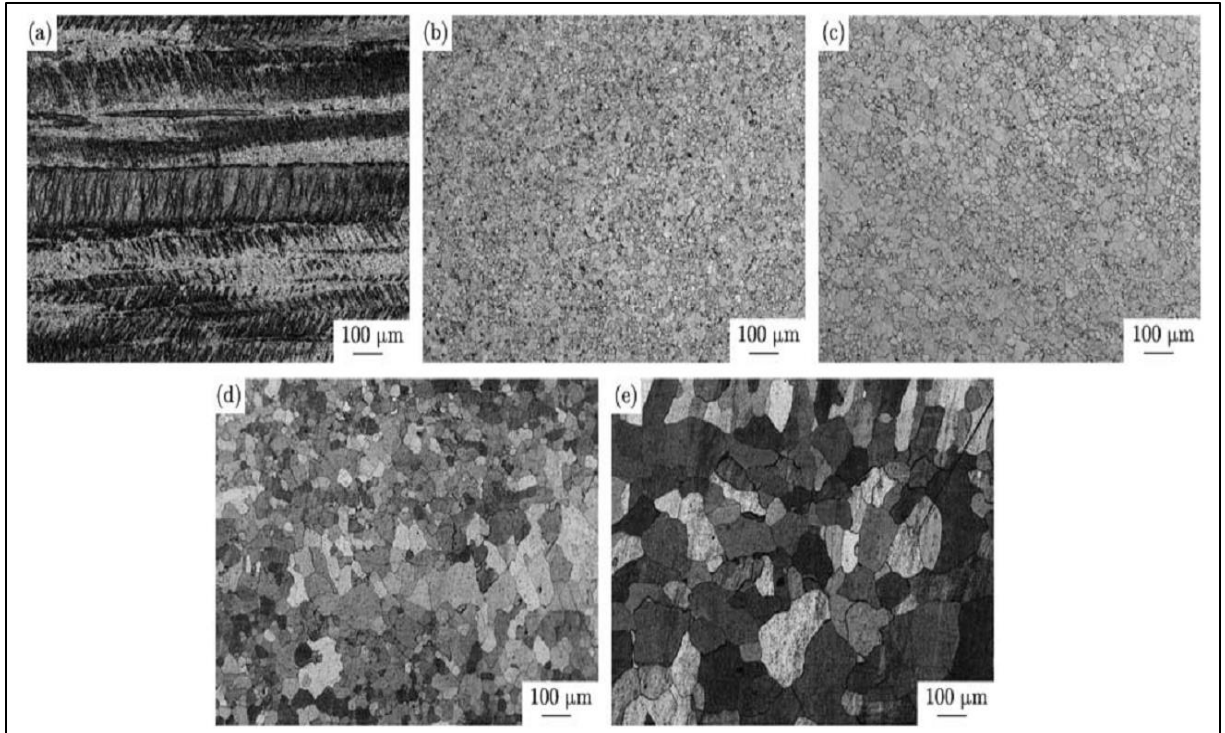


Figure 20: Photomicrographs of Ferritic SS New obtained after annealing at different times at 1100 °C: (a) 0 min; (b) 5 min; (c) 10 min; (d) 30 min; (e) 60 min [61]

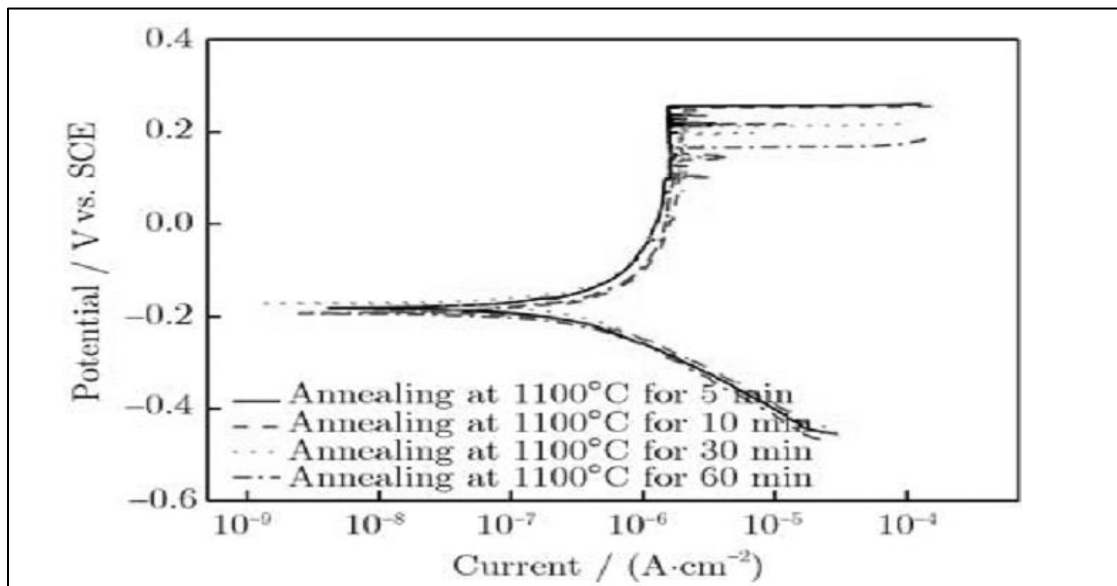


Figure 21: Anodic polarization curves of Ferritic stainless steel samples with different annealing times in a 3.5 w t % NaCl solution.[61]

Samples were processed for eight passes using a MoS₂ lubricant at 500 °C which were pressed at a speed of 4 mm/s. Before equal channel angular process, sample grain size was measured to be 50µm. ECAP process reduced the grain size from 80-120 nm.

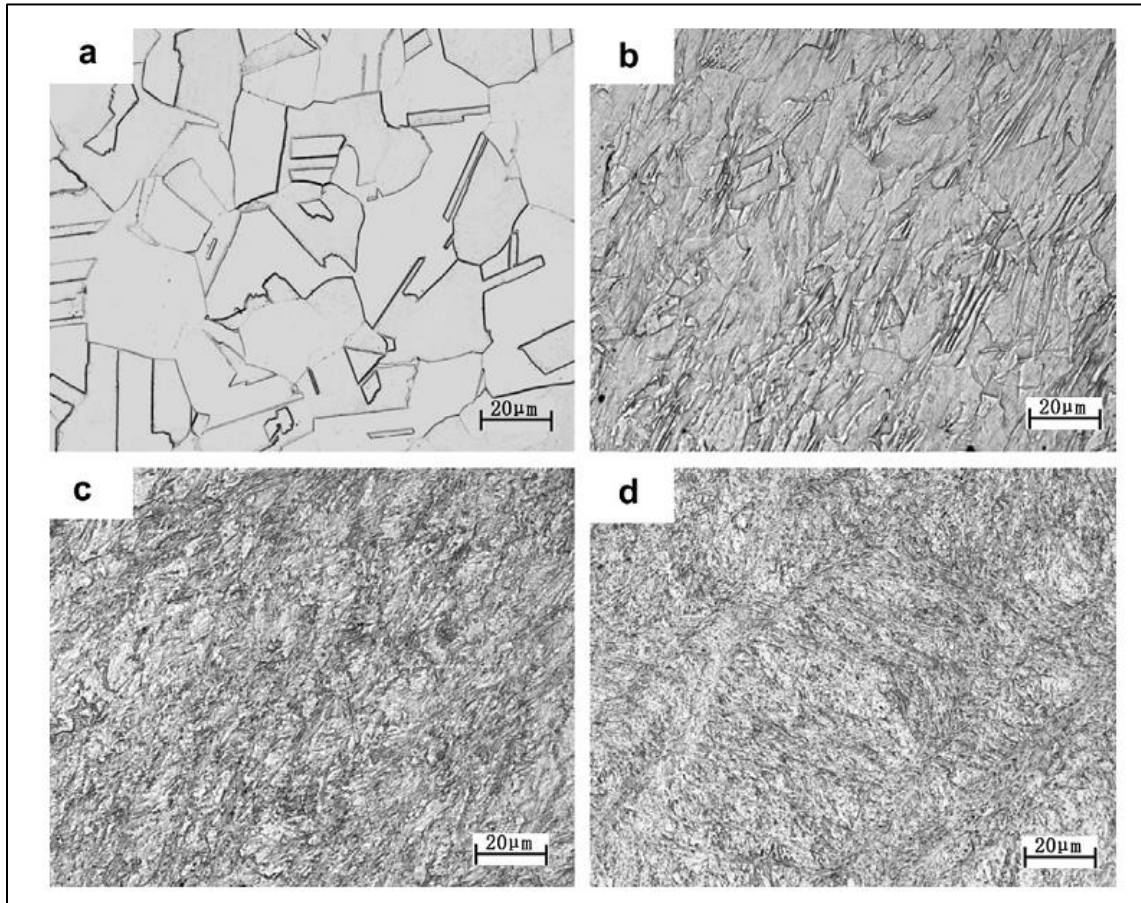


Figure 22: Photomicrographs of as-received and ECAPed 304 SS after different passes: (a) (0 pass), (b) 1 pass, (c) 4 pass (d) 8 pass [62]

ECAPed SSs samples were analyzed by using electrochemical tests to determine the corrosion properties. Testing was carried out in 0.5M H₂SO₄ solution. The potentiodynamic polarization curves observed in all the samples has same shape (Figure 23). The corrosion potentials of the samples in polarization curves were found to be varying a lot. Polarization curves further revealed that the corrosion properties of 304 SS

was improved when the grain size has been reduced to 80-120nm by using ECAP process.

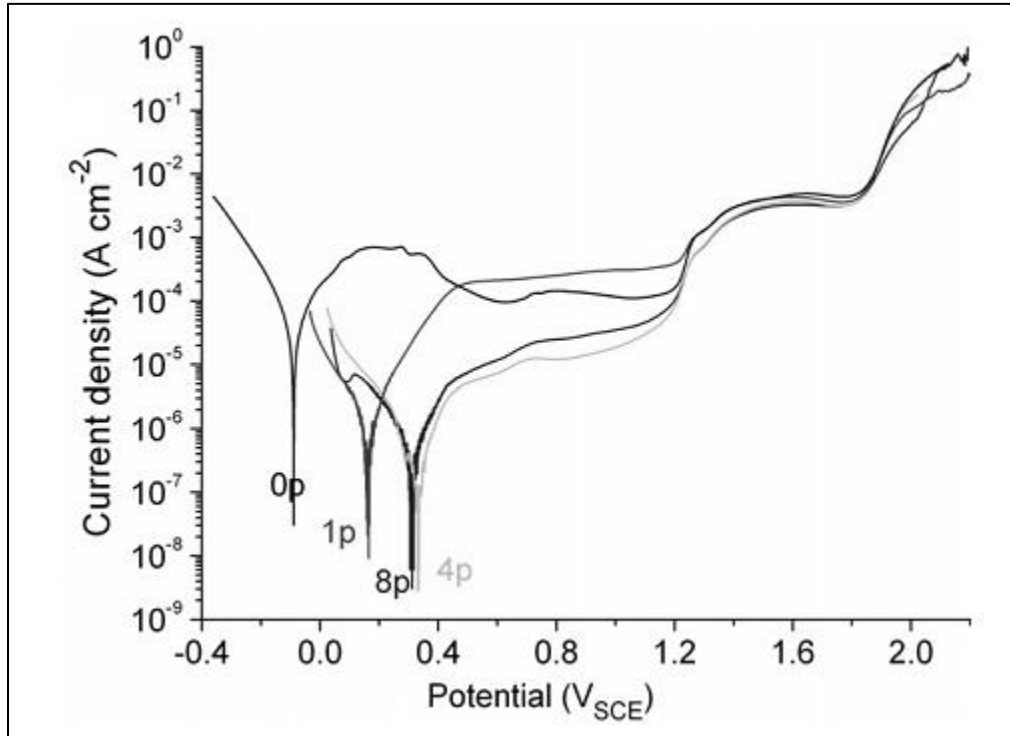


Figure 23: Potentiodynamic polarization curves of samples with and without ECAPed SS in 0.5 M H₂SO₄ solution [62]

Electrochemical impedance spectroscopy was also used to study the electrochemical characteristics of 0, 1, 4 and 8 pass samples. Nyquist plots of general and ECAPed samples at open circuit potential in 0.5M H₂SO₄ solution are shown in Figure 24. The Nyquist plots revealed that the as-received and single pass samples have smaller and depressed semicircle as compared to the diameters of 4 and 8 pass samples. The 4 & 8 pass samples showed larger diameter depressed capacitive semicircles in high-frequency region. The increased diameter of semi-circle indicates an increase in passive film stability. EIS studies revealed that finer grains size samples had the best and stable passive layer.

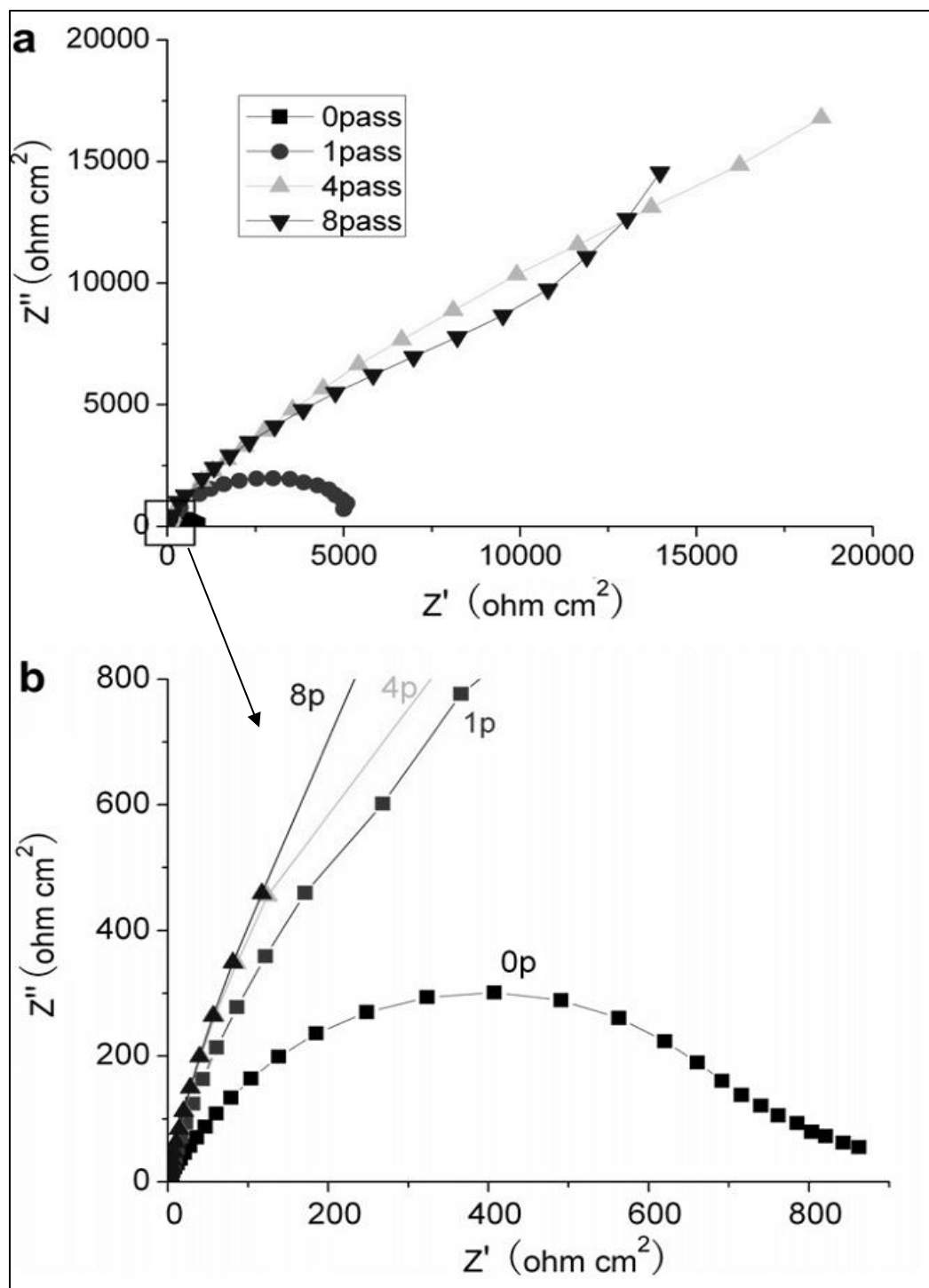


Figure 24: (a) Nyquist plots general and ECAPed samples and (b) magnified graph for the small black area in (a) [62]

CHAPTER 3

MOTIVATION AND OBJECTIVES OF THE RESEARCH

The proper selection of materials and investigation can predict corrosion and cut down the losses incurred due to corrosion. Different alloys were developed to provide better corrosion resistance for certain corrosive environments. Usually, Ni alloys and SSs are used in industry for corrosion resistance. With the evolution of the industry and development of industrial practices, the operating conditions of the industry are becoming more and more challenging to the materials to keep their integrity intact. Hence, development of new alloys which not only provide better corrosion resistance but are also economical are of prime importance. Among all SSs, Ferritic SSs are probably the most widely used structure materials. The reason for this extensive use in the industry is because of their resistance to localized corrosion i.e pitting and intergranular corrosion. However, despite of their extensive application in industry, the equipment manufactured of steels exhibits poor service quality. Inexpensive corrosion-resistant materials are more and more needed nowadays because of the ever increasing environmental corrosivity. This poses the aim of searching for new, effective but not scarce alloying elements. Si may be one of them since it conventionally ranks among the elements that stabilize α -modification of iron. Si is always present in the killed steel at an amount of 0.2–0.3%. Presence of over 0.3–0.4%, Si is referred to as an alloying element that reduces the carbon solubility in Ferrite and improves the alloy's hardness and strength as a consequence of the drastic distortion of the Fe crystal lattice.

By now, numerous Fe–Si-system-based steels are developed. The most known of them are containing 1.0 to 4.5% Si and acid resistant containing 12–18% Si. Their properties

are determined by the formation of a thick and dense film of silicon–iron mixed oxide at the alloy surface. However, these steels are extremely brittle and can stand neither hot nor cold work. Adaptability of Fe–Si alloys to manufacture is improved significantly upon introducing such elements as Cr, V, and Nb. Therefore, low-alloy and stainless steels are used as structural materials wider than Fe–Si alloys. In particular, adding 1.0–1.6% Si to low-alloy chrome steel ($C_{Cr} = 1.3\text{--}12\%$) results in its strengthening, stabilizing against tempering, somewhat improved hardening, and an increase in the corrosion resistance

In most of the studies, researchers used mostly commercial stainless steels when they were studying electrochemical properties. Their samples mostly contain Si along with other alloying elements such as Mo, Cu, etc. As every alloy addition has different effect, so it becomes very difficult to understand the real effect of Si on the corrosion resistance of SSs. In order to understand the real effect of Si, no other alloy addition should be added and the electrochemical properties then must be compared.

The purpose of this study was to

- ❖ Design and develop **Fe-18Cr-XSi (X=0-4)** alloys
- ❖ Investigate the effect of Si the corrosion properties of the **Fe-18Cr-XSi (X=0-4)** by using different electrochemical techniques
- ❖ Investigate the effect of grain size on the electrochemical properties of **Fe-18Cr-XSi (X=0-4)** by using different solution annealing times.

CHAPTER 4

MATERIALS AND METHODOLOGY

4.1. Alloy Development

Fe-18Cr-XSi (X=0, 2, 4 wt. %) alloys were prepared by using a vacuum arc melting process, after which the casting is done in the form of buttons. After that, hot rolling operation was performed and 6mm thick samples were obtained, the thicknesses of the samples were further reduced to 3mm via cold rolling. Samples were solution annealed for 30 and 60 minutes at 1050 °C. Chemical analysis of the samples is shown in table 1.

Table 1: Chemical Composition of Ferritic Stainless Steels Samples

	Chromium (%)	Silicon (%)	Iron
1	18.33	0.11	Balance
2	17.29	2.52	Balance
3	16.76	4.43	Balance

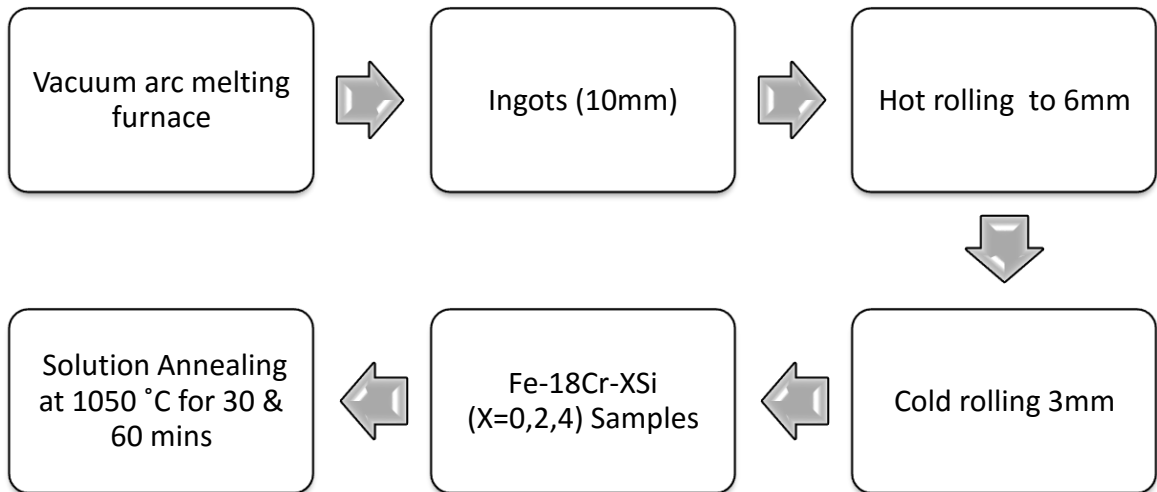


Figure 25: Shows process flow chart for Fe-Cr alloy production

4.2. Specimen Characterization

For metallurgical assessment, samples were cut into the dimension of 1cm x 1cm. Samples were then hot mounted after which the samples were fine grinded up to 1200 grit silicon carbide paper. Polishing was carried out by using 1 μ m diamond paste followed by etching in Marble's reagent to distinguish the grain boundary for morphology observation. In order to detect grain boundary carbides, samples were electrolytically etched as per the guidelines provided in ASTM A763 [63]. Etching solution used was 10% Oxalic acid and the current of 1 A cm⁻² was applied for 1.5 minutes during the etching process. Metallurgical examination was carried out by Nikon Eclipse MA200 microscope equipped with a camera connected to a computer. Grain size was measured after different annealing time periods by following the guidelines of ASTM E112 [64] Direct Comparison Method. For Electrochemical assessment, copper wire is attached to the samples followed by cold mounting. The surface of the samples was finely grinded up to 600 grit size. Polishing was done by using alumina paste followed by sonication up to 10 min.

4.3. Electrochemical Investigations

The Electrochemical investigations were carried out on 30 and 60 minutes annealed samples in 0.5M NaCl and (0.1M NaCl + 0.1 M H₂SO₄) solutions respectively. Gamry Reference 3000 was used as a potentiostat. A conventional 3 electrode system as shown in Figure 26 was used with sample under investigation acting as a Working Electrode, graphite as a Counter Electrode and Saturated Calomel Electrode (SCE) as a Reference electrode. Potentiostat is an instrument which controls the voltage difference between a sample under investigation and a Reference Electrode. Counter electrode is used to pass

current in the electrochemical cell. In almost all applications, the potentiostat measures the current flow between the working and counter electrodes. The reference electrode in the cell was connected to the corrosion solution through a Luggin capillary bridge. Potential was swept at a scan rate of 0.5 mV sec^{-1} in the applied potential range from -0.8 V to 1.4 V . The surface area exposed to test solution was 0.2 cm^2 and all the experiments were carried out at room temperature. Before proceeding with the potentiodynamic scans, samples were immersed in solution for 15 minutes in order to stabilize open circuit potential (OCP). Corrosion potential (E_{corr}) and corrosion current (I_{corr}) values were determined by using Tafel extrapolation. Electrochemical Impedance spectroscopy (EIS) was carried out by scanning from higher to lower frequencies with the applied frequency range of 0.01 Hz - 100 KHz . Amplitude of the applied sinusoidal wave was 10 mV . Echem Analyst software was used for data fitting of the impedance spectra. Linear polarization experiments were performed by polarizing the specimen from $+15$ to -15 mV with respect to E_{corr} . Samples were scanned at the rate of 0.5 mV sec^{-1} .

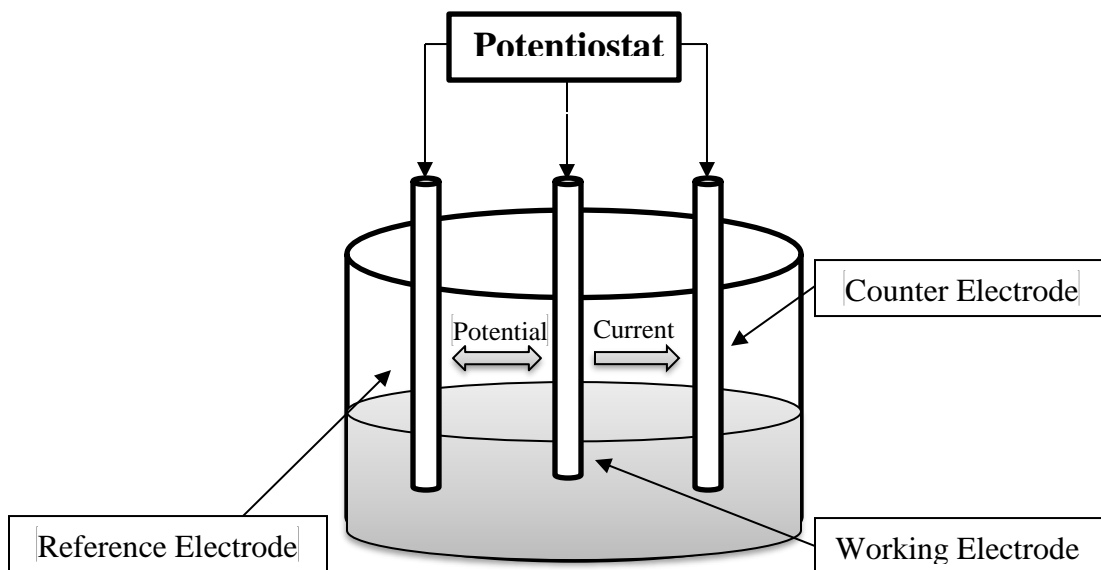


Figure 26: Schematic of polarization test apparatus (Potentiostat is connected with 3 electrode electrochemical cell)

CHAPTER 5

RESULTS & DISCUSSION

5.1. Microstructural Examination

In order to understand the microstructure of the material, microstructure analysis of the samples were carried out at different magnifications. Photomicrographs in Figures 27 & 28 revealed the microstructure of Fe-18Cr-XSi samples after annealing at 1050 °C for 30 and 60 minutes. General microstructure of all the samples revealed fully Ferritic structure. Grains were found to be equiaxed in nature.

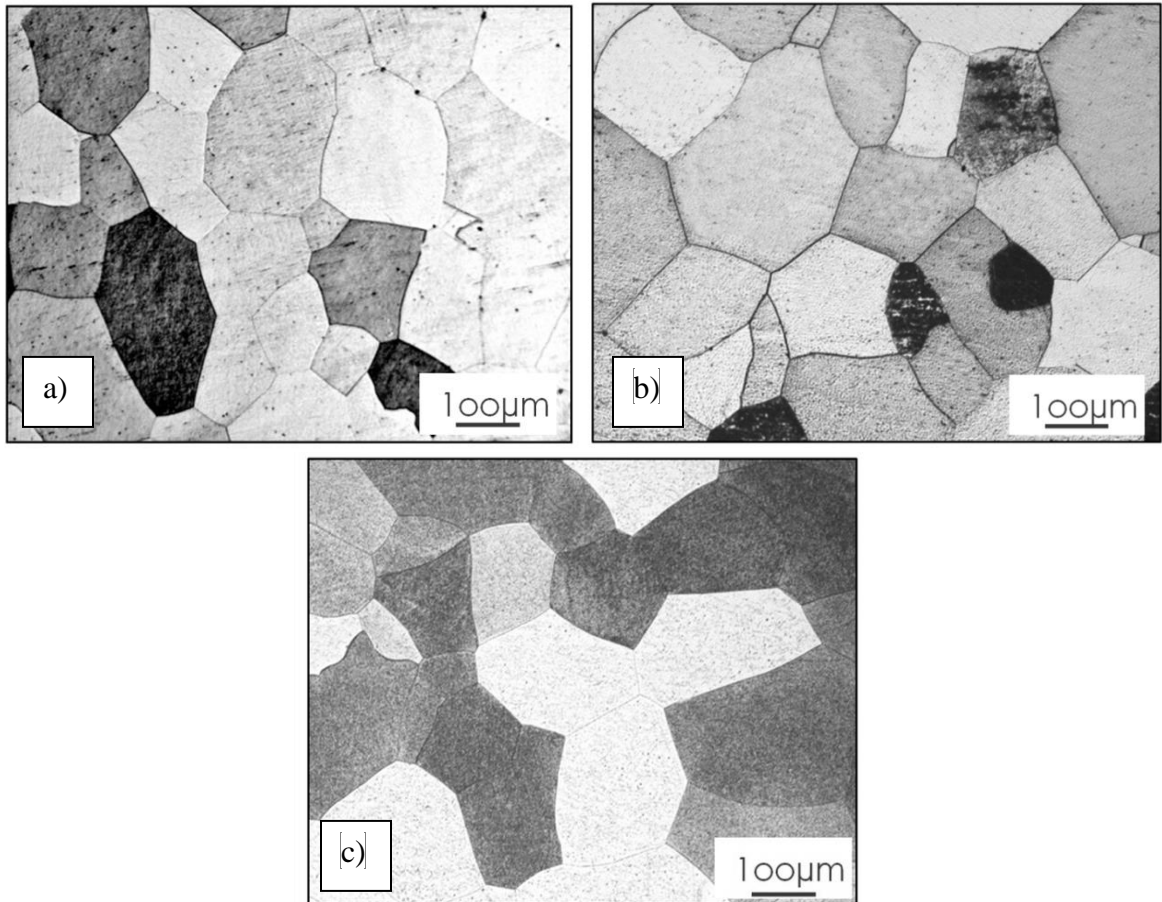


Figure 27: Microstructures of the alloys a) Fe-18Cr-0Si b) Fe-18Cr-2Si and c) Fe-18Cr-4Si annealed for 30 minutes

In order to measure the grain size, ASTM E112 method was employed and microstructure at 100x magnification was compared with the ASTM Grain size chart Plate 1B.

Plastically deforming a material requires certain amount of energy. The amount of energy applied will be stored in the material in the form of internal energy due to which there will be some changes produced in physical and mechanical properties. Usually, when the material is cold worked, the hardness increases with the amount of cold working applied. The internally stored energy in the material increases dislocation density and point defects density. At a microstructural level, grain becomes elongated and heavily distorted. As the hardness is increased due to cold working so, it is often important to return the material to its original condition and this process is called annealing. In annealing the cold worked material is held at a temperature above the 1/3rd of the melting point for a specific period of time. In annealing the recovery is the first step in which the point defects are reduced and dislocations within the material are rearranged which result in the formation of subgrains and their boundaries and reduced hardness. The next stage is the recrystallization stage in which nucleation and growth will take place in the deformed matrix. At this stage the dislocations are further annihilated at the boundaries of the newly formed grains. After recrystallization, if the material is annealed for a longer period of time then the grain growth usually occurs. Grain boundaries between annealed grains migrate and coarser grains develops and grow which in turns increase average grain size (Grains become coarser) and reduction in hardness is observed [65].

For Ferritic SSs, annealing is the only possible heat treatment as there will be no phase transformation that will occur for this family of SSs during heat treatment. In Ferritic

SSs, annealing is carried out to optimize the corrosion properties by uniformly distributing the Cr content in the microstructure.

For different grades, different annealing times and duration can be selected keeping in mind the purpose of annealing. Ferritic SSs are sensitive to grain growth so selection of specific temperature and holding time is required to get desired grain size. After annealing, thin products with higher Cr content are always cooled in air to avoid embrittlement at 475°C. So, in this research, annealing was carried out not only to recrystallize the microstructure after cold rolling but also to achieve coarser grains.

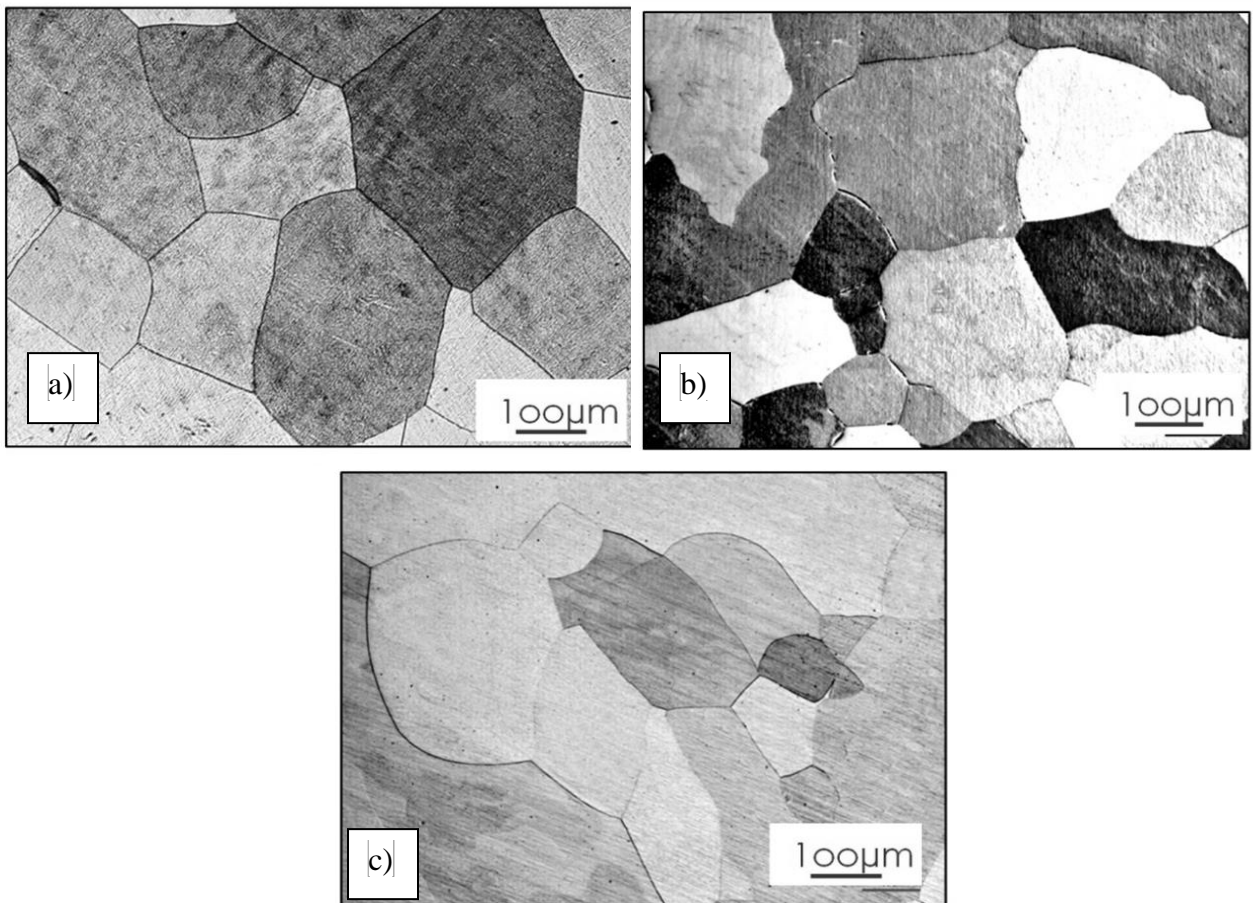


Figure 28: Microstructures of the alloys a) Fe-18Cr-0Si b) Fe-18Cr-2Si and c) Fe-18Cr-4Si annealed for 60 minutes

Equiaxed Ferrite grains were observed in three compositions after annealing for 30 and 60 min at 1050°C. Average Grain size in all the samples was found to be approximately 226 μm for 30 minutes annealed sample and 320 μm for 60 minutes annealed sample. From microstructural study and grain size analysis, it was observed that by increasing the annealing time the grain size becomes coarser as compared to the grain size in lower annealing time samples.

5.2. Identification of Chromium Carbide Formation

Intergranular corrosion (IGC) is one of the important form of localized corrosion. In IGC, localized corrosion occurs in the vicinity of grain boundary area which is depleted with Cr content. This depletion is caused by the formation of carbides at the grain boundaries. As the affinity of Cr to C is high so, when given a favorable temperature, Cr will react with C and will form chromium carbides and intermetallic phases at the grain boundaries. This phenomenon of carbide precipitation at the grain boundaries is called “Sensitization”. Due to carbide precipitation, area adjacent to the grain boundaries becomes depleted with Cr and becomes potential site for corrosive attack due to unfavorable anode to cathode ratio. When sensitized SSs encountered highly oxidizing conditions, the corrosive ions attack the grain boundaries and accelerated cracking occurs along the grain boundaries.

IGC is a common problem in Austenite SSs however, in Ferritic SSs, sensitization also occurs due to the formation of carbides at the grain boundaries. The temperatures required for carbide precipitation is lower in Ferritic SSs as compared to Austenitic SSs (Figure 29) however, the carbide precipitation times are very short. To improve resistance

to IGC, Ferritic SSs must be annealed which will properly disperse the chromium towards the chromium depleted zones [66].

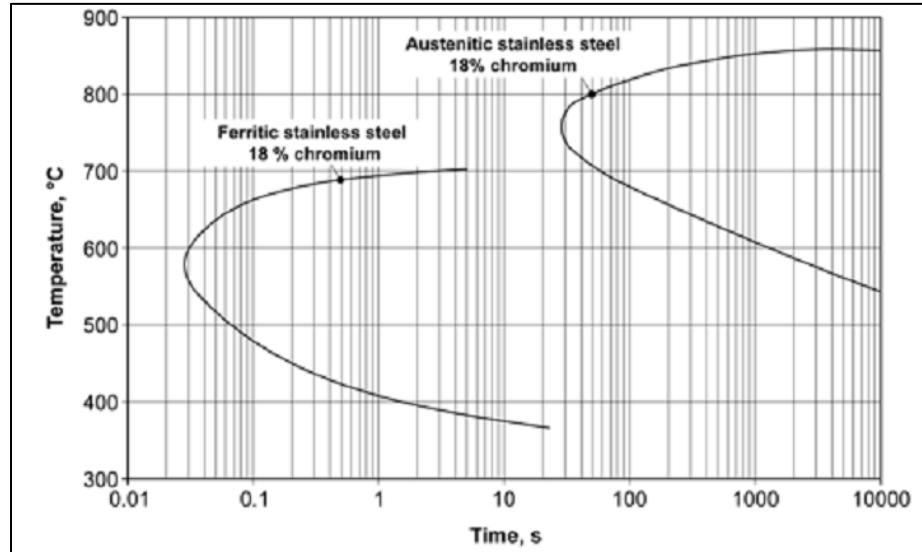


Figure 29: Sensitization curve of Ferritic & Austenitic SSs [66]

In this research, samples were subjected to different annealing times. In order to make sure that there is no carbide precipitation, the samples were electrolytically etched as per the guidelines provided in ASTM A763 practice W which is a standard to detect susceptibility of Ferritic SSs to IGC. Two different types of microstructures exist in the standard, one without any carbide precipitation (step structure Figure 30) and other with grain boundary carbide precipitation (Ditch structure Figure 31). After etching the samples, microstructures were observed under the microscope at different magnifications. No carbide precipitation along the grain boundaries (Step structure) was observed which can have a negative influence on the corrosion properties of the alloys. The results obtained from this test (Figure 32) revealed that the samples are not susceptible to intergranular corrosion (IGC).

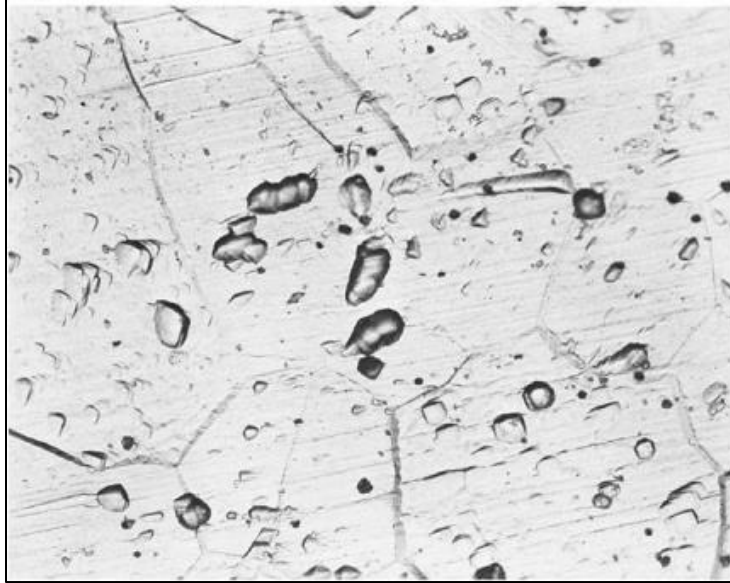


Figure 30: Steps between grains; Acceptable structure with no grain boundary carbides [63]

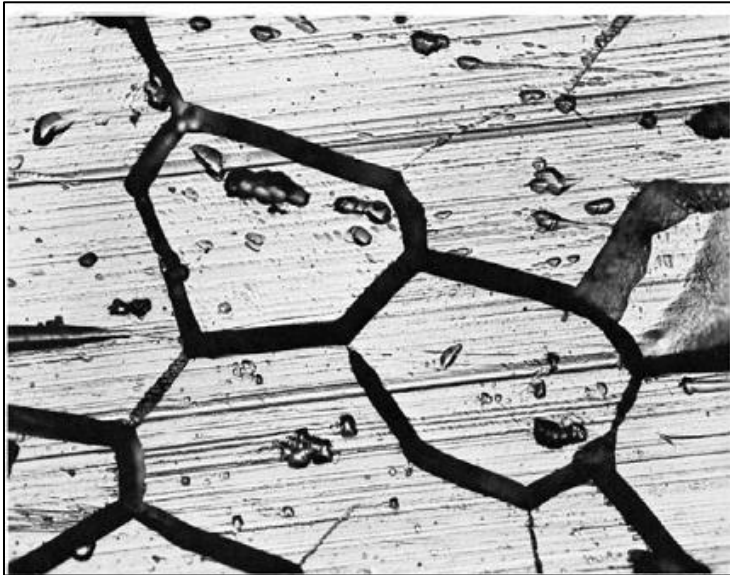


Figure 31: Ditched structure; Unacceptable structure with grain boundary completely surrounded by carbides [63]

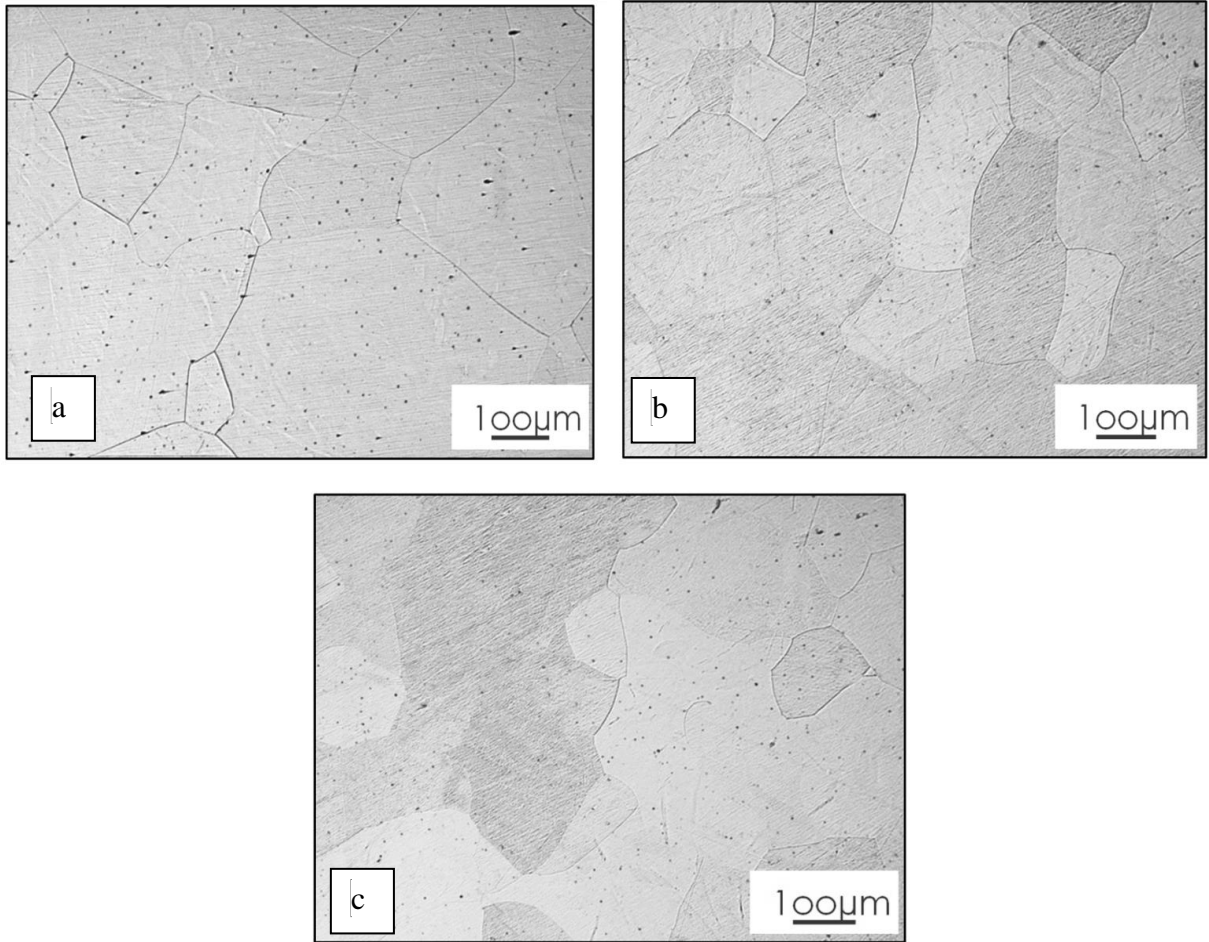


Figure 32: Microstructures of the alloys a) Fe-18Cr-0Si b) Fe-18Cr-2Si and c) Fe-18Cr-4Si obtained after ASTM A763 (IGC) test. No ditches at grain boundaries were observed

5.3. Localised Corrosion Behaviour of Fe-18Cr-XSi (X=0-4)

5.3.1. Potentiodynamic Polarization (PDP) in 0.5M NaCl Solution

Potentiodynamic polarization (PDP) scan provide useful information of electrode processes like the passivity of the alloy, corrosion rate in a specific environment, pitting susceptibility of the alloy etc. The rate at which the anodic or cathodic reactions are occurring on the sample under investigation (working electrode) is represented by current in a potentiodynamic experiment. Current in the potentiodynamic test is represented in terms of current per unit area of the working electrode, also called current density. There are different variables which can have an influence on the electrochemical reaction rate

which includes temperature, sample surface condition and the experimental environment. Usually, cathodic currents are negative and anodic currents are positive.

In potentiodynamic scans, the anodic part is of a great importance as it can be used to get different parameters of the electrochemical system. Figure 33 shows the anodic and cathodic part of the potentiodynamic spectra. Anodic scan starts from point A and progresses in the positive (potential) direction until termination at point B. Most notable features on the curve are the open circuit potential which is located at point 1. At this potential the sum of the anodic and cathodic reaction rates on the electrode surface is zero and the current will be closed to zero value. Point 2 depicts the passive potential / passive current density which is indication of the formation of passive film on the surface of the sample. The point 3 then shows that with increase in potential there is no or small increase in current density which states that the reaction rate is reduced and metal dissolution occurred. This region is also called passive range. Now, as the potential values reached to a specific value for an alloy the current density starts to increase rapidly. This increase in current density is attributed to the localized dissolution of the passive film and this region is also called a transpassive region (point 4).

The Corrosion potential E_{corr} and Corrosion current I_{corr} are usually calculated from Tafel extrapolation method in which the linear region of the anodic and cathodic regions are extrapolated to a point where the anodic and cathodic reaction rates are equivalent. These points will give the values of corrosion current density (i_{corr}) and corrosion potential (E_{corr}).

Figure 33 & Table 2 shows the results obtained from Potentiodynamic Polarization (PDP) experiments for Fe-18Cr-XSi (X=0-4) samples annealed for 30 minute in 0.5 M NaCl

solution. Passive region was observed in all the samples tested where current density is almost constant. Polarization curves also show that, once the pitting potential is reached, the current density increases sharply, this abrupt increase indicates the breakdown of the passive film. The breakdown of the passive film was due to the dissolution of the alloy and can be linked to a localized corrosion phenomenon called pitting. After the experiment visual examination of the sample surfaces also revealed pits throughout surface.

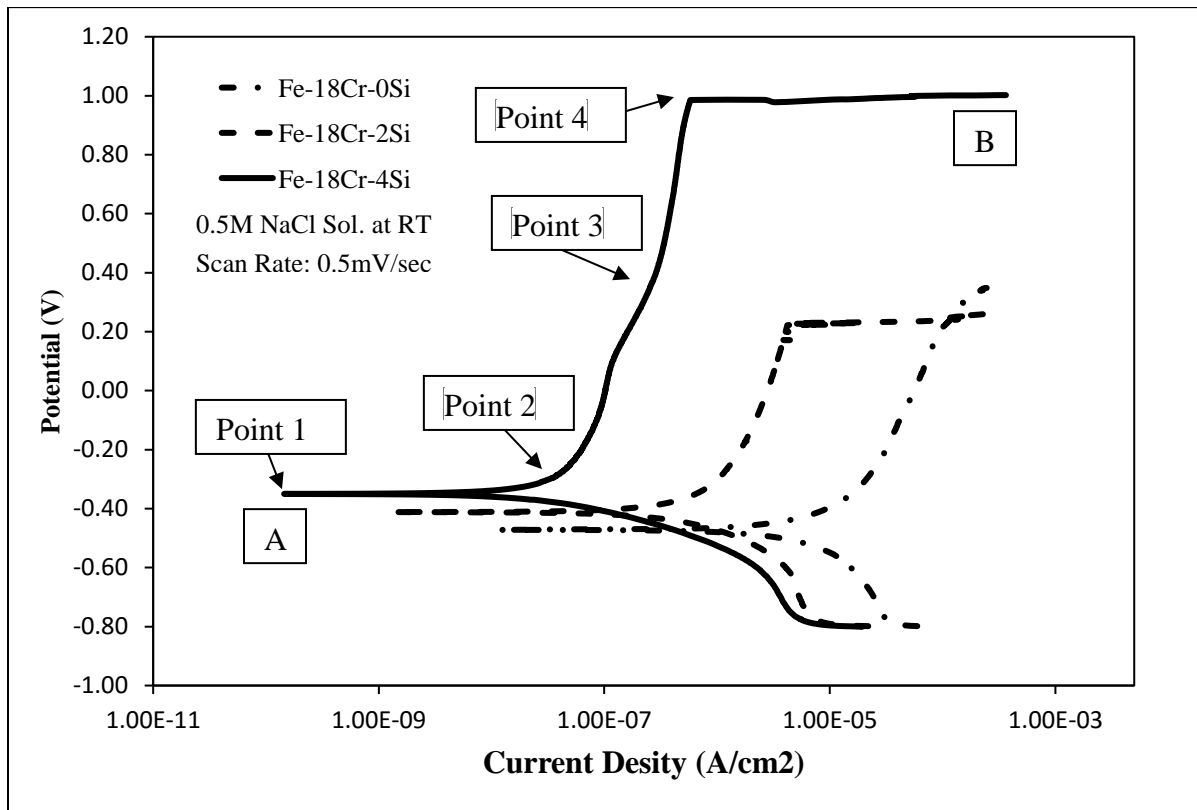


Figure 33: Polarization curves obtained in 0.5M NaCl solution for 30minutes annealed samples.

The polarization spectrum for sample containing 0 wt. % Si (Fe-18Cr-0Si) shows highest value of passive current density ($i_{pass} = 23.2 \mu A$) as well as lowest pitting potential ($E_{pit} = 197.9mV$). Due to low pitting potential values, passive region was significantly less as compared to other samples containing 2 & 4 wt. % Si. The curves of sample with 4wt.%

Si (Fe-18Cr-4Si) shows lowest passive current density ($i_{\text{pass}} = 0.05 \mu\text{A}$) when compared with the values of sample containing 0 and 2 wt.% Si. The only difference between the samples was the silicon content which can be a sole reason for improved electrochemical properties.

Highest active potential was also observed for sample containing 0 wt. % silicon with $E_{\text{corr}} = -472 \text{ mV vs SCE}$. Figure 33 also indicates that with the addition of silicon, the Corrosion Potential (E_{corr}) improved. The best E_{corr} -350 mV value was observed for sample containing 4 wt. % Si. The pitting potential E_{pit} , is an important factor to study localized corrosion resistance of stainless steels. The addition of 4 wt. % Si in the alloy increases the E_{pit} values from 197.9 mV to 985.7 mV which means that sample with 4wt.% Si has the more stable and longer passive region.

Table 2: Summary of potentiodynamic polarization (PDP) experiments in 0.5MNaCl

Electrolyte		0.5M NaCl		
Sample	E_{corr} (mV)	i_{corr} (nA)	E_{pit} (mV)	I_p (nA)
0Si	-472	1.9	197.9	23.22
2Si	-412	1.2	226.3	1.58
4Si	-350	0.03	985.7	0.05

5.3.2. Potentiodynamic Polarization (PDP) in Acidic Chloride Solution (0.1M NaCl+ 0.1M H₂SO₄)

Acidic Chlorides are present in different industrial environments like marine, pressure vessels, offshore oil and gas production, power, plants etc. The acidic chloride can also be found in the localized corrosion areas such as in pits or crevices where the corroded

area contains chloride and hydrogen ions in abundance. Because of the oxidizing power and the presence in different applications where SSs is widely used, it was decided to include this medium in the electrochemical studies.

In acidic chloride environments, sample behaves differently when compared with only chloride containing solutions. In polarization spectra, an extra region in the anodic curve was observed which depends on the oxidizing condition of the electrolyte. After open circuit potential is reached, the increase in potential shifts the anodic curve in the active region. In this region, the oxidation of the sample is the major reaction that is taking place. The current density at the start of the region is called critical current density (i_c) which depicts the start of the passive film formation and when the current density is further reduced the stable passive film is achieved in the passive region. When anodic curve shows this kind of behavior then it means that, there is no spontaneous passivation taking place, instead, material is behaving in both active and passive manner. In this case, in the active region, metal dissolution has to occur to develop stable passive film.

The electrochemical properties of Fe-18Cr-XSi (X=0-4) alloys were also tested in (0.1M NaCl+ 0.1M H₂SO₄) solution. Figure 34 and Table 3 shows the summary of results and polarization curves.

Polarization spectra shows that for all the 3 composition tested (Fe-18Cr-XSi (X=0-4), there is not any appreciable difference in the values of the corrosion potential (E_{corr}) however the corrosion potential was observed to more negative in sample with 4 wt.% Si (Fe-18Cr-4Si) as compared to sample with 0 wt.% Si(Fe-18Cr-0Si). The critical current density values also revealed the same trend as the sample with 4wt.% Si shows slightly higher i_c values as compared to samples with 0 & 2 wt.% Si.

Figure 34 also indicates that addition of Si does not make any major difference to the corrosion potential and critical current density in acidic chloride solution and reason might be the extra grain boundary attack. All the samples achieved passivity with different values of passive current density i_p . The passive current density values revealed that the sample with 4 wt.% Si shows lower values as compared to other samples. Passive range was also found to be wider in 4wt. % Si sample with higher pitting potential.

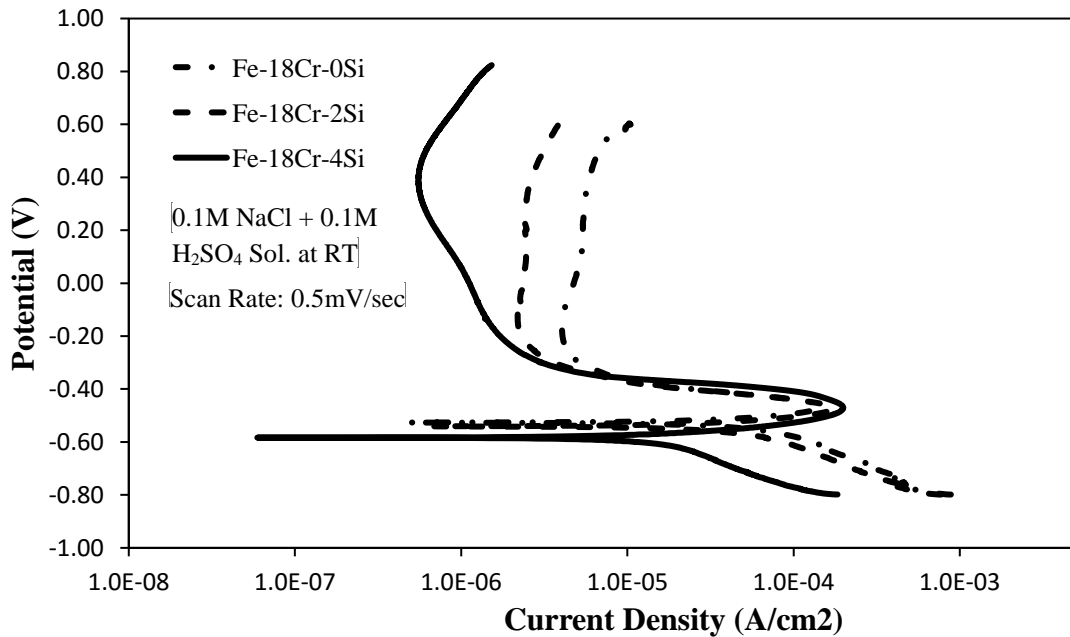


Figure 34: Polarization curves in 0.1M NaCl+ 0.1M H₂SO₄ solution for 30minutes annealed samples

The main trend that had been observed from polarization experiment is that, with increasing Si content in the Fe-18Cr alloy the electrochemical properties becomes better. i.e the sample with 4 % Si has the best passive current density and pitting potential. This same trend has also been observed when these alloys were tested in 0.5M NaCl solution.

Table 3: Summary of potentiodynamic polarization (PDP) experiments in 0.5MNaCl and 0.1M NaCl+ 0.1M H₂SO₄ solution for 30 min. annealed samples

Electrolyte	0.1M NaCl+ 0.1M H ₂ SO ₄				
Sample	E _{corr}	i _{corr}	E _{pit}	i _p	i _c
	(mV)	(nA)	(mV)	(μ A)	(μ A)
0Si	-527	225.1	503.1	4.13	144.7
2Si	-541	68.6	643.9	2.26	171.7
4Si	-583	22.4	823.9	1.38	196.4

Improvement in the passive current density can be linked to the property of Si that it promotes anodic dissolution in the active range as observed by many authors [29, 67]. Blajiev et al. [29] investigated the effect of Si on the corrosion behavior of Fe-25Cr Ferritic SSs with 1-5 wt. % of Si in 1 Normal sulfuric acid solution. It was reported that, Si when added upto 5%, accelerates anodic dissolution, slows down the cathodic reaction, and facilitates transition to the passive state. Kasparova et al. [67] studied the influence of Si on the electrochemical properties of Fe-Cr Alloy by using Mössbauer spectroscopy. It was observed that, addition of 5 % Si in the Fe-Cr alloy accelerates the anodic dissolution in the active range and improves the passivation ability in the range of active–passive transition.

Different E_{pit} values in all the samples were also observed in the current research in both the solutions. The positive effect of Si on E_{pit} of SSs is due to the formation of more stable oxide film at higher potentials. The large passive region and higher E_{pit} values achieved by 4 wt. % Si addition are the evidence of the stable passive film and may have been possibly linked to the formation of two layered structure. Most of the Si content is

present on the surface layer as SiO_2 / Faylite and chromium layer containing Cr_2O_3 is located on the metal matrix as reported by Hoi et al. [31]. Hoi, investigated the effect of Si by using potential decay curve and used X-Ray photoelectrons spectroscopy (XPS) for surface film analysis. It was reported that, Si addition promotes two layered structure in the passive film. Tasi et al. [68] also studied the effect of Si on sintered 304 SSs. It was observed that the formation of SiO_2 layer on the sample surface helps in improving the corrosion resistance. Robin et al. [69] correlated the composition of the passive layer to the corrosion resistance of SSs with Si content. The XPS studies of the passive layer revealed silicon to be present in the passive layer in large amounts. Toor et al. [70] investigated the effect of Si content on 304 and 304Si SSs and reported pronounced effect of Si on the E_{pit} and i_{pass} of the alloy. So, from the discussion above we can infer that the presence of Si in the passive layer along with Cr makes it more compact and form a barrier that prevents the transferring of metal ions from passing into solution hence the corrosion resistance found to be greatly improved.

5.3.3. Electrochemical Impedance Spectroscopy (EIS) in Chloride Solution (0.5M NaCl)

Different techniques have been developed to characterize electrochemical systems. Electrochemical impedance spectroscopy (EIS) is one of the popular and a powerful technique to study different parameters of the electrochemical systems. Resistance offered to the flow of electrical signals is called Impedance of the circuit which consists of the combination of resistance, capacitance and inductance. In EIS, alternating current (AC) of small amplitude is applied on the sample under investigation (Working electrode) and resistance to current flow is measured in terms of impedance.

Two types of graphs can be obtained in EIS i.e. Nyquist plot and the Bode plot. In Nyquist plot the real and imaginary part of the impedance is plotted. The impedance of the system is measured at different frequency. The real impedance is plotted on X axis and the imaginary part is plotted on Y axis. A capacitive loop is obtained in this plot which shows different parameters like solution resistance, polarization resistance and nature of the electrochemical reactions i.e. charge transfer or mass transfer. Right side of the plot shows impedance at lower frequency and left side of the plot revealed impedance at higher frequencies. In Bode Plot, impedance is plotted with log frequency on the X-axis and log of impedance or phase-shift on the Y-axis. Bode Plot shows frequency information at each and every point of the plot.

In order to confirm the positive effect of Si on Fe-18Cr alloy with Si addition, Impedance studies were carried out at open circuit potential (OCP) in 0.5M NaCl solution. Figure 35 & 36 shows Nyquist and Bode plot for 30 minutes annealed samples. All samples showed similar impedance features when they were analyzed in 0.5 M NaCl solution. In Nyquist plot, the simplest way to determine the corrosion properties of the samples is by comparison of semi-circle diameters. The larger the diameter better will be the corrosion resistance [71]. In Nyquist plot (Figure 25) a capacitive depressed semi-circle was observed for all the samples from high to intermediate frequencies but with appreciable variation in diameters. There is deviation observed from pure semi-circle behavior and it is attributed to roughness and inhomogeneity of the surface film. [72]. The capacitive arc in Nyquist plot for sample with 4 wt. % Si consists of partial circle with indefinite radii and did not intersect X axis at any point. This behavior is related to highly capacitive character of passive materials and is also indicated by the phase angle v/s frequency plot

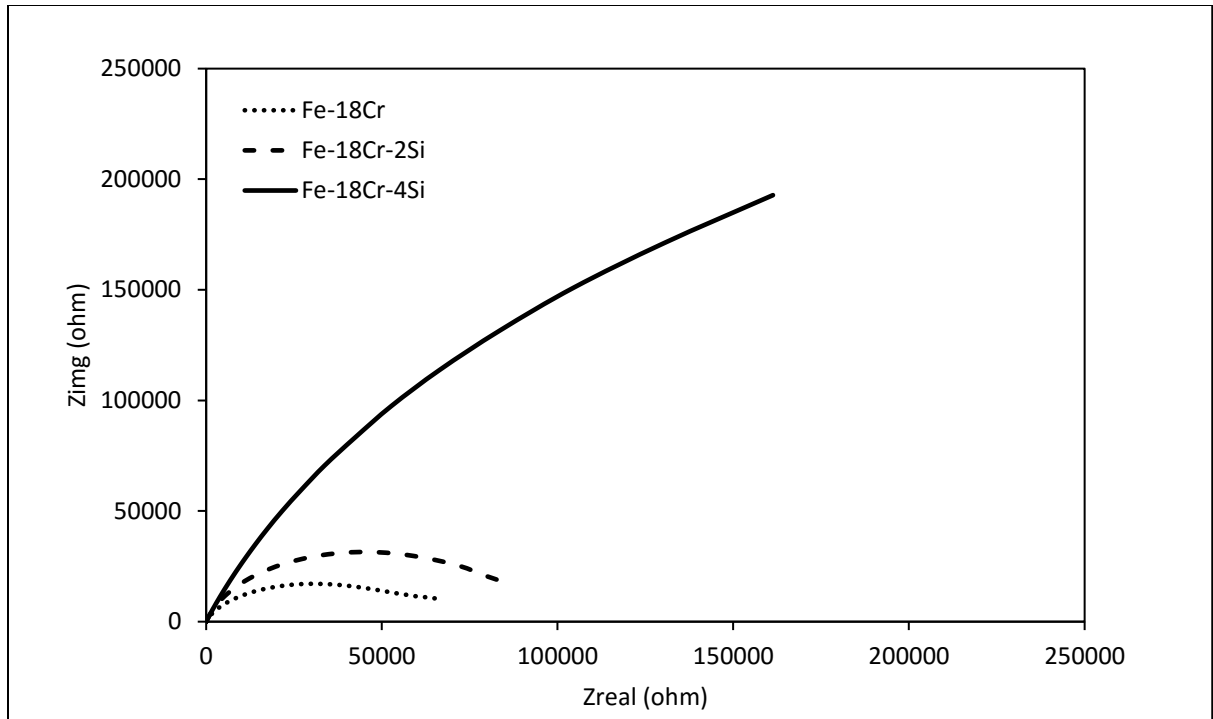


Figure 35: Nyquist plot in 0.5M NaCl solution for 30 minutes annealed samples

In phase angle vs. frequency plots (Figure 36) a peak is observed at high to intermediate frequencies and a valley is observed at low frequencies, which represent the capacitive character. The presence of the capacitive loop can be attributed to charge transfer reaction from the alloy into the electrolyte through the double layer capacitance, and the diameter of the semi-circle is related to the charge transfer resistance (R_{ct}) at the metal/solution interface. Phase angles for all the samples were in the range of -70° which indicate that all the samples achieved passivity. The phase angle is approaching -70° from intermediate to low frequencies which indicate the presence of stable and strong passive film.

After data acquisition, an impedance spectrum was fitted by a circuit model shown in Figure 37 by using Echem Analysts software. As discussed earlier, In Fe-Cr alloys passive film formed has duplex nature which consists of an inner chromium oxide layer

which is in contact with the metal substrate and an outer surface layer of iron oxides and hydroxides which is in contact with the electrolyte.

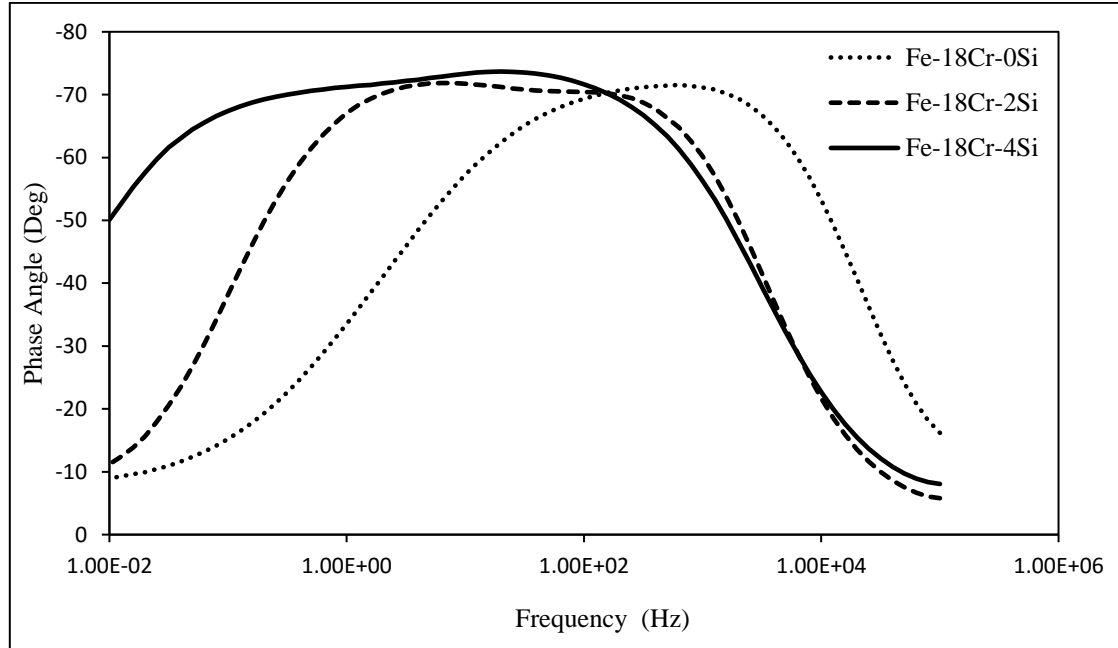


Figure 36: Bode plot in 0.5M NaCl solution for 30 minutes annealed samples

Based on literature, it was suggested to use a two layered model for curve fitting and explanation of EIS data [73, 74]. In the circuit, R_s corresponds to solution resistance; R_f represents the resistance of surface layer resulted from film defects; R_{ct} is the charge transfer resistance of film/steel interface. The CPE_f and CPE_{dl} are the constant phase elements at the film-solution and substrate-solution interfaces, respectively.

Values of porous film resistance R_f , R_{ct} and R_s were calculated after curve fitting. Resistance polarization R_p of the passive film was calculated by addition of R_f and R_{ct} . When the frequency response of the system is not ideal then to model the behavior of passive film a constant phase element (CPE) was used in the circuit. Impedance of CPE can be calculated by using following equation

$$Z_{cpe} = Y^{-1}(j\omega)^{-n} \quad (1)$$

Where $Y = C = \text{capacitance}$, j is $\sqrt{-1}$, ω is the frequency and $-1 < n < 1$ is phase shift. For non-homogenous system CPE is used instead of a capacitor.

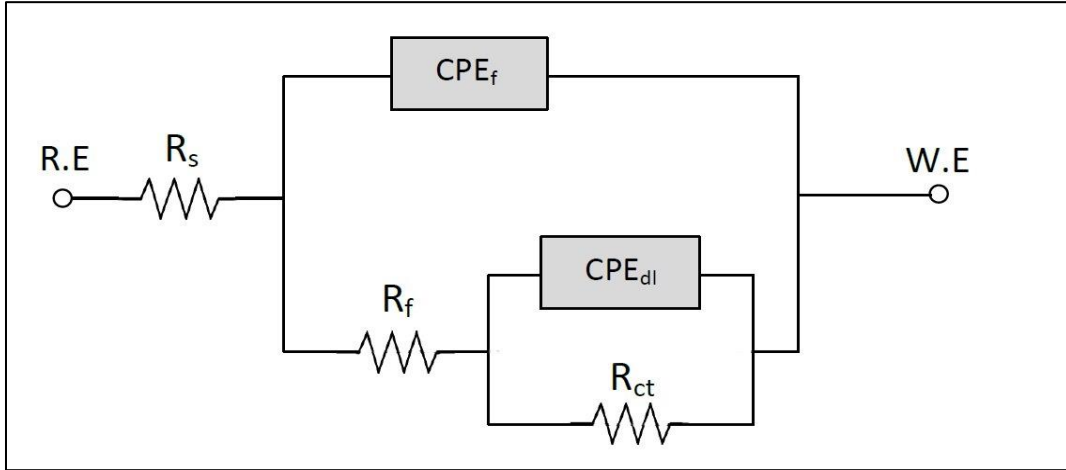


Figure 37: Two layered model used to fit the impedance curves of Fe-18Cr-XSi samples

Constant phase element was used to model the role of imperfect capacitor. The use of CPE can also be explained by referring to the values of “ n ” in Table 4. The values are in between 0-1 which confirms that passive film is not a perfect capacitor.

From Nyquist plot, it is observed that with the addition of Si, diameter of the semi-circle increased. Different charge transfer resistance values were obtained after curve fitting as shown in Table 4. The differences in the values were because of the different dissolution rates in each sample due to the chemical composition of the alloy. The highest charge transfer resistance (R_{ct}) was observed in sample containing 4wt.% Si (Fe-18Cr-4Si) which shows lowest susceptibility of the material in chloride environment. R_p value is calculated by adding the resistance offered by two layers and it is interesting to note that

most of the resistance came from the barrier layer as was observed by other researchers [75, 76]. Sample with 4 wt.% Si achieved the highest R_p value (661.5 KOhm.cm^2) which further states that passive film formed has the highest protective ability due to the synergistic of Si and Cr in the passive layer.

Table 4: EIS parameters obtained in 0.5M NaCl solution for 30 min. annealed samples after curve fitting

Sample No.	Si (%)	R_s ($\Omega.\text{cm}^2$)	R_f ($\text{K}\Omega.\text{cm}^2$)	CPE_f (F.cm^{-2})	N_f	R_{ct} ($\text{K}\Omega.\text{cm}^2$)	C_{dl} (F.cm^{-2})	N_{dl}	R_p ($\text{K}\Omega.\text{cm}^2$)
1	0	18.08	1.5	$2.1\text{e-}6$	0.8	83.54	$8.24\text{e-}6$	0.3	85.04
2	2	20.50	8.1	$17.9\text{e-}6$	0.8	100.1	$4.7\text{e-}6$	0.2	108.2
3	4	18.57	0.07	$29.6\text{e-}6$	0.8	661.50	$1.25\text{e-}6$	0.4	661.57

5.3.4. Electrochemical Impedance Spectroscopy (EIS) in Acidic Chloride Solution (0.1M NaCl+ 0.1M H₂SO₄)

EIS studies were also conducted in (0.1 M NaCl + 0.1 M H₂SO₄) solution in order to find the response of acidic chloride environment as was done by different researchers[77, 78]. Figures 38 & 39 shows Nyquist and Bode plot for Fe-18Cr-XSi(X=0-4) alloy in (0.1 M NaCl + 0.1 M H₂SO₄) solution.

All samples showed similar impedance features. Capacitive depressed semi circles were observed in Nyquist plot for all the samples from high to intermediate frequencies but their diameters were different due to different impedance response of the samples. Sample with 0 wt.% Si(Fe-18Cr-0Si) showed smaller diameter semi-circle as compared to diameter of the sample containing 4wt.% Si. In sample with 4 wt.% Si, the semi-circle at high frequencies did not intersect at X axis at any point so this nature of the impedance

curve can be related to the capacitive character of passive materials and is also indicated by the phase angle v/s frequency plot. The phase angle is approaching -70° from intermediate to low frequencies which indicates the presence of stable and strong passive film which probably consists of Cr_2O_3 , Fe_2O_3 , SiO_2 and a spinel faylite. Phase angles for all the samples were in the range of -60 to -70 degrees which indicates the formation of passive film.

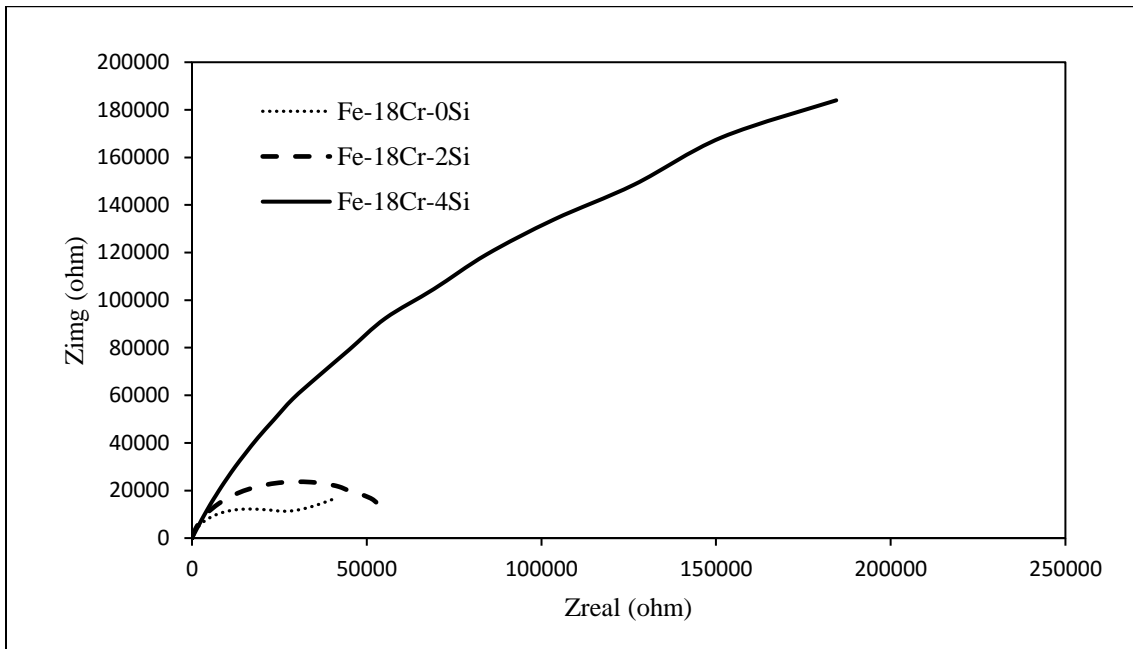


Figure 38: Nyquist plot in 0.1M NaCl+ 0.1M H₂SO₄ solution for 30 minutes annealed samples

Same Circuit model as discussed earlier has been used to fit impedance curves. In order to model the behavior of non-ideal systems, Constant phase element was used instead of a capacitor to model the capacitive behavior of the film. 'n' values listed in Table 5 also confirms the imperfect capacitance of the film because values are in the range of 0-1. Charge transfer resistance R_{ct} was found to be increasing as the Si content is increased in the samples. Highest R_{ct} value was observed for sample with 4 wt.% Si (Fe-18Cr-4Si)

which further helps the theory that with increasing Si content in Fe-18Cr alloys the passive film present on the alloy becomes more stable and highly protective because of the synergistic effect of Cr and Si present in the film.

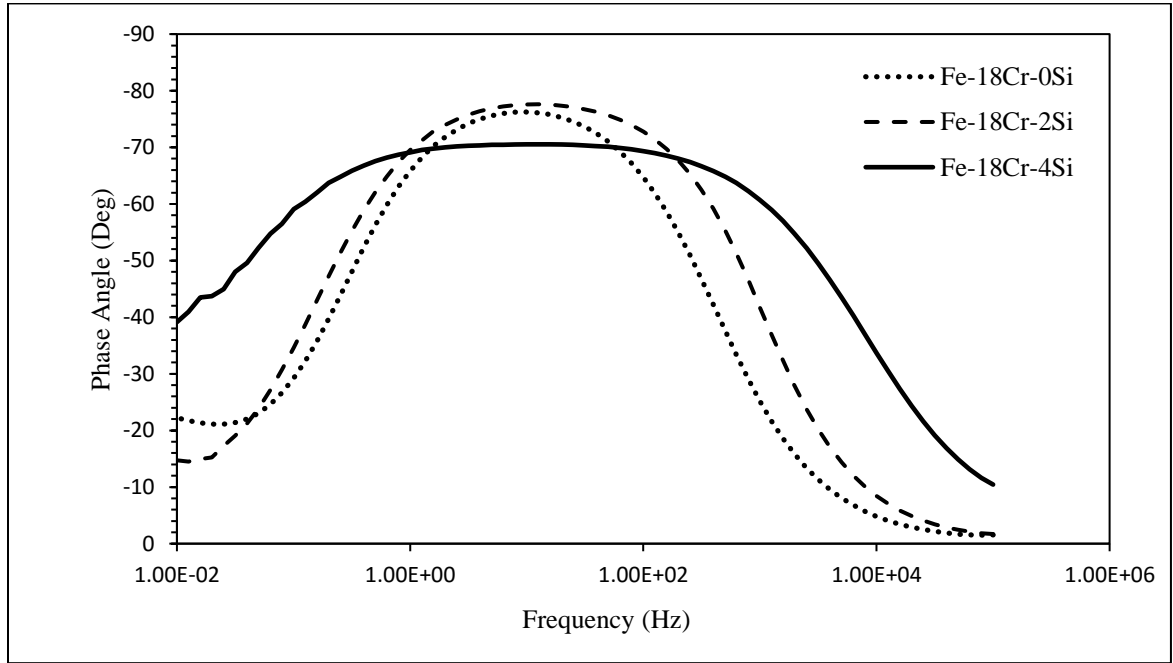


Figure 39: Bode plot in 0.1M NaCl+ 0.1M H₂SO₄ solution for 30 minutes annealed samples

Table 5: EIS parameters obtained in 0.1M NaCl + 0.1M H₂SO₄ solution or 30 min. annealed samples after curve fitting

Sample No.	Si (%)	R _s (Ω.cm ²)	R _f (KΩ.cm ²)	CPE _f (F.cm ⁻²)	N _f	R _{ct} (KΩ.cm ²)	C _{dl} (F.cm ⁻²)	N _{dl}	R _p (KOhm.cm ²)
1	0	24.51	32.4	29.3e-6	0.8	21.35	63.5e-6	0.9	53.7
2	2	19.77	0.02	19.5e-6	0.8	58.1	0.9e-6	1.0	58.1
3	4	17.44	0.03	8.29e-6	0.7	581.5	3.95e-6	0.7	581.5

5.4. Linear Polarization Resistance (LPR)

Linear polarization resistance (LPR) is a non-destructive and quick technique to get data from corroding system. In doing so, the sample under investigation is polarized in the

order of $\pm 10\text{mV}$ relative to Open Circuit potential which is the measured potential when no current is flowing. Current will flow between the sample and counter electrode when the potential of the system is changed. Resistance polarization of the sample can be found by taking the slope of the potential versus current curve

The principle of LPR is explained when a metallic sample is immersed in an oxidizing solution, the electrochemical reactions will take place and material will corrode. During corrosion process, anodic and cathodic reactions are taking place and flow of electrons from anode to cathode generate corrosion current which can be used to get the resistance polarization values by using Stern Gary equation.

The polarization resistance (R_p) of the metal mainly depends on the passive film formed on the surface [79] and is the direct measure of corrosion resistance of the material. Data obtained from linear polarization experiments is shown in Table 6 for 0.5M NaCl and (0.1M NaCl + 0.1M H_2SO_4) solutions. R_p value of sample containing 4wt. % Si was found to be higher as compared to R_p values of sample containing 0 & 2 wt. % Si. It is clearly evident from the results that, as the Si content increases; polarization resistance also increases this is due to the fact that the presence of Si in the passive layer makes it more stable. The R_p values found in LPR test and EIS test are quite different which can be explained by the fact that time taken by EIS experiment is more as compared to LPR which is a very quick method . The more time the sample stays in the solution the more will be differences in the electrochemical parameters. The same trend has been seen in the acidic chloride solution as well. The results obtained in LPR test also confirms / strengthen the results obtained in PDP and EIS experiments.

Table 6: LPR data in 0.5M NaCl & 0.1M NaCl+0.1M H₂SO₄ solution for 30 min. Annealed samples

Electrolyte	0.5M NaCl	0.1M NaCl+0.1M H₂SO₄
Silicon (%)	Resistance Polarization R_p (KΩ)	Resistance Polarization R_p (KΩ)
0	4.9	4.1
2	173.9	161.1
4	492.8	461.3

5.5. Effect of Grain Size on Electrochemical Properties of Fe-18Cr-XSi Alloys

In this research, the effect of grain size on the electrochemical properties was also investigated. In order to find the effect of grain size, two different annealing times were selected and samples were annealed for 30 and 60 minutes respectively. Microstructure analysis revealed that the grains become relatively coarser when the annealing time was increased from 30 minutes to 60 minutes as expected. 60 minutes annealed samples were then subjected to electrochemical analysis as was done on 30 minutes annealed sample to compare the corrosion properties.

5.5.1. Effect of Grain Size on Localized corrosion resistance (Potentiodynamic polarization experiments)

Potentiodynamic polarization experiments were performed in 0.5M NaCl solutions for sample annealed for 60 minutes. Passive region was observed in all the samples tested where current density is almost constant showing spontaneous passivation. Polarization curves also show that, once the pitting potential is reached, the current density increases

sharply, due to the dissolution of the alloy. Pits were observed on the surface after the experiments.

Sample with 0 wt. % Si (Fe-18Cr-0Si) showed highest value of passive current density as well as lowest pitting potential as compared to sample with 2 & 4 wt.% Si. The lowest passive current density was observed for sample with 4wt,% Si (Fe-18Cr-4Si). The highest pitting potential E_{pit} was observed in the sample containing 4 wt.% Si and the passive region was also found to be wider as compared to other samples. The addition of 4 wt. % Si in the alloy increases the E_{pit} values from 44.1 mV to 541.5 mV which means that sample with 4wt.% Si has the more stable and longer passive region. Here, the only difference between the samples was the silicon content which can be a sole reason for improved electrochemical properties. Similar trend had been observed in the sample annealed for 30 mins as explained in section 5.3.1.

Now, to compare the PDP results of 30 min annealed sample and 60 min annealed samples, all the PDP curves were combined. Figure 40 shows combined potentiodynamic curves and electrochemical data of 30 and 60 minutes annealed samples in a 0.5 Molar NaCl solution. From Figure 40 and Table 7 It were observed that the coarser grain size samples (60 min. annealing) have higher passive current densities when compared with the 30 min. annealed samples with relatively finer grain size. The Pitting potential values were found to be on the lower side in 60 min. annealed samples as compared to 30 min. annealed samples. Pitting potential values decreased with increasing the annealing time and the passive range becomes smaller.

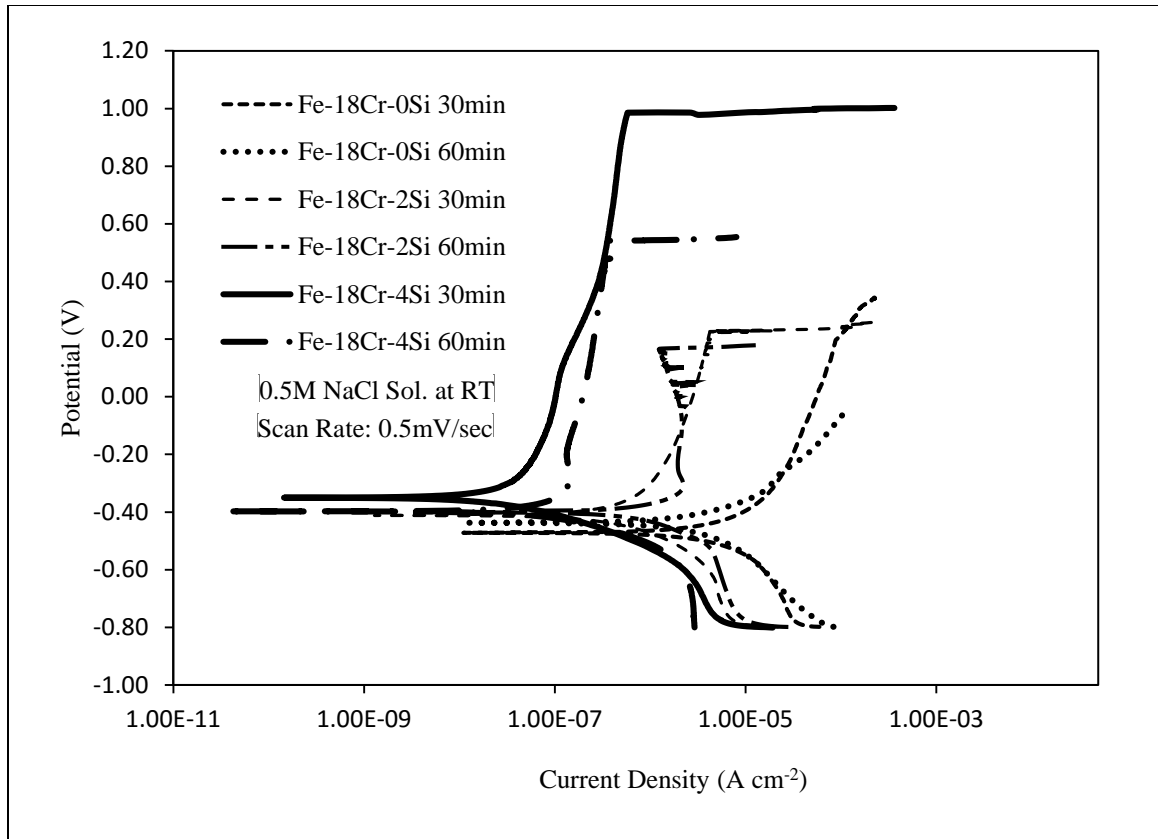


Figure 40: Combined Polarization curves in 0.5M NaCl solution for 30 and 60 min. annealed samples

The largest passive range was observed for sample with 4% Si which was annealed for 30 min. and having relatively finer grain size. The similar effects of grain size on corrosion resistance were observed by L.Jinlog et al. [80] Effect of grain size on alloy 690 was investigated by reducing the grain size to 280nm. It was observed that the ultrafine grain size sample exhibits lower passive current density and higher pitting potential as compared to coarse grain size samples. The same author [81] also investigated the effect of grain size on 2205 Duplex SS. The ultrafine grain size sample revealed reduced passive current density and higher pitting potential as compared to coarse grain size sample.

Table 7: Summary of potentiodynamic polarization (PDP) experiments in 0.5MNaCl solution for 30 and 60 min. annealed samples

Electrolyte	0.5M NaCl solutionfor 30 and 60 min.annealed Samples			
Sample	Ecorr (mV)	icorr (nA)	Epit (mV)	Ip (nA)
0Si – HT 30	-472	1.9	197.9	23.22
0Si – HT 60	-437	3.7	44.1	30.3
2Si – HT 30	-412	1.2	226.3	1.58
2Si – HT 60	-400	1.9	166.6	2.17
4Si – HT 30	-350	0.03	985.7	0.05
4Si – HT 60	-398	0.07	541.5	0.14

The electrochemical properties of Fe-18Cr-XSi (X=0-4) alloys were also tested in (0.1M NaCl+ 0.1M H₂SO₄) solution for 60 min. annealed samples. Polarization spectra revealed active-passive behavior of the samples as was also observed in the samples annealed for 30min. due to higher oxidizing power of the acidic chloride solution. The critical current density values were found to be low for sample with 4wt.% Si as compared to samples with 0 & 2 wt.% Si. The low critical current density means that passive film is developing at low current density values. The passive current density values were also found to be on the lower side in sample with 4 wt.% Si. Passive range was also found to be wider in 4wt. % Si sample with higher pitting potential values. The PDP results also complimenting the trend that was observed in 30 min. annealed samples that increasing the Si content in the samples enhances corrosion properties.

Combined PDP spectra for samples annealed at 30min and 60min in (0.1 M NaCl + 0.1 M H₂SO₄) solution are show in Figure 41 and the summary of the polarization data obtained from PDP curves is shown in Table 8.

From Figure 41 and Table 8 it was observed that 60 min. annealed samples with coarser grains size had higher values of i_{crit} and i_{pass} as compared to 30 min. annealed samples with relatively finer grains size. The pitting potential values for 60 min. annealed samples were found to be on the lower side which means the coarser grains had negative effect on the pitting potential values.

The results of the comparison of the samples with different annealing times in different environments, it was found that coarser grain size due to longer annealing times had impart overall negative effect on the electrochemical properties.

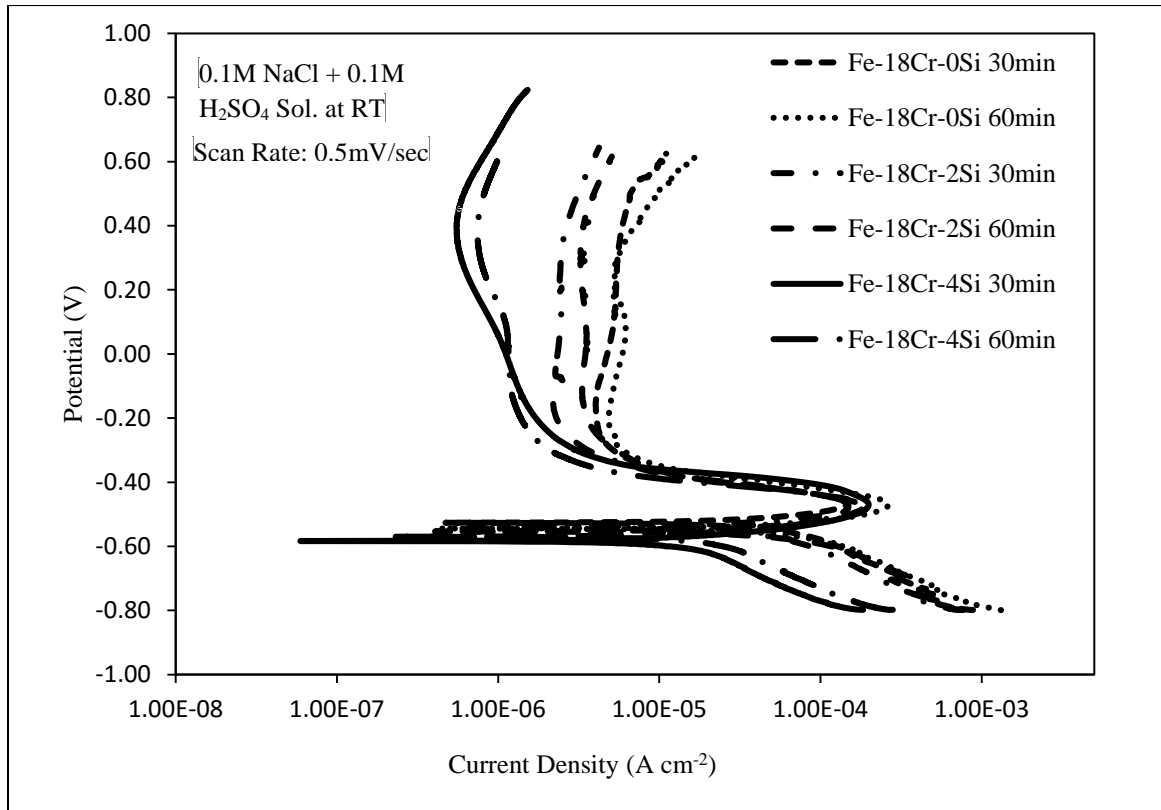


Figure 41: Combined Polarization curves in 0.1M NaCl+ 0.1M H₂SO₄ solution for 30 and 60 min. annealed samples

Table 8: Combined potentiodynamic polarization (PDP) experimental data obtained in 0.5M NaCl & 0.1M NaCl+ 0.1M H₂SO₄ solution for 30 & 60 min. annealed samples

Electrolyte	0.1M NaCl+0.1M H ₂ SO ₄ Solution for 30 and 60 min.annealed Sample				
Sample	E _{corr} (mV)	I _{corr} (nA)	E _{pit} (mV)	I _p (nA)	I _c (ua)
0Si – HT 30	-527	225.1	503.1	4.13	144.7
0Si – HT 60	-545	254.0	303.1	4.93	262.1
2Si – HT 30	-541	68.6	643.9	2.26	171.7
2Si – HT 60	-549	110.0	595.0	3.44	184.0
4Si – HT 30	-583	22.4	823.9	1.38	196.4
4Si – HT 60	-570	41.4	603.1	1.39	147.0

5.5.2. Effect of Grain Size on Electrochemical Impedance Spectroscopy (EIS) Spectra in Chloride and Acidic Chloride Solution

Impedance studies were also carried out at open circuit potential (OCP) in 0.5M NaCl solution for 60 min. annealed samples. The impedance curves showed that all samples have similar impedance features. In Nyquist plot (Figure 42) a capacitive depressed semi-circle was observed for all the samples from high to intermediate frequencies but the diameters were varying with the composition of the samples. Pure capacitive loops were not observed which can be linked with roughness and inhomogeneity of the surface film. The capacitive arc in Nyquist plot for sample with 4 wt. % Si consists of partial circle with indefinite radii and did not intersect X axis at any point. This behavior is related to highly capacitive character of passive materials. The presence of the capacitive loop can be attributed to charge transfer reaction from the alloy into the electrolyte through the double layer capacitance, and the diameter of the semi-circle is

related to the charge transfer resistance (R_{ct}) at the metal/solution interface. Same circuit as shown in Figure 37 was used to fit the curves and Echem analyst software used to acquire data. Table 9 shows the summary of the data. The highest charge transfer resistance (R_{ct}) was observed in sample containing 4wt.% Si (Fe-18Cr-4Si) which shows lowest susceptibility of the material in chloride environment. R_p value is calculated by adding the resistance offered by two layers. Sample with 4 wt.% Si achieved the highest R_p value (550 KOhm.cm^2) which further states that passive film formed has the highest protective ability due to the synergistic of Si and Cr in the passive layer. Similar trend had also been observed by L. Jinlong [80]. EIS studies in the research on ultrafine alloy 690 samples revealed higher impedance values with a large diameter semi-circle as compared to coarse grain sample. It was reported that the ultrafine grain size sample shows higher charge transfer resistance and it was attributed due to the grain refinement. L. Jinlong [81] in his other research also found the charge transfer resistance to be high in fine grained 2205 Duplex SS as compared to coarse grain sample. Balusmay [82] also conducted research on AISI 490 SSs by modifying the surface by achieving grain size in nanometers. It was reported in the research that surface nanocrystallization promotes passive film formation and increases the corrosion resistance. For comparison purpose the EIS curves were superimposed and shown in Figure 42. Table 8 shows electrochemical data obtained after curve fitting. After comparison of EIS spectra of 30 and 60 min. annealed samples it was found that, resistance polarization values for samples annealed for 60 min. with coarser grain size was less as compared to the values of 30 min. annealed samples with finer grain size. This means that the resistance offered

by the passive film to charge transfer in coarser grain size was less as compared to finer grain samples.

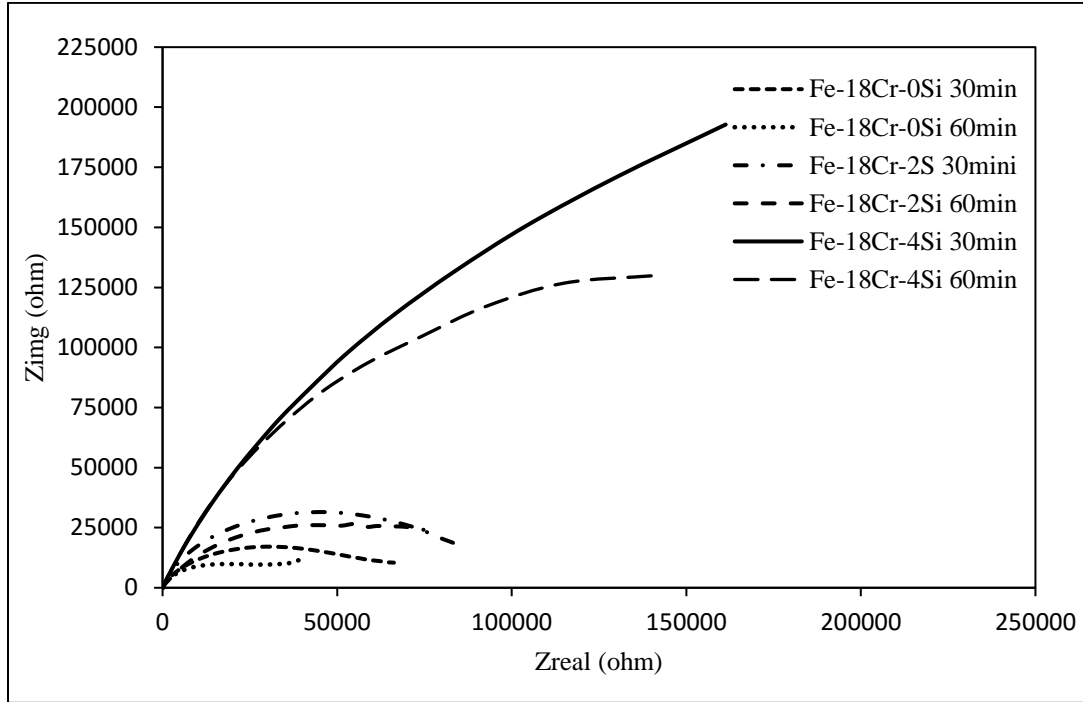


Figure 42: Combined Polarization curves in 0.5M NaCl solution for 30 and 60 min. annealed samples

Table 9: Combined EIS parameters obtained in 0.5M NaCl solution for 30 & 60 min. annealed samples after curve fitting

Annealing Time	Si (%)	R_s ($\Omega.cm^2$)	R_f ($K\Omega.cm^2$)	CPE_f ($F.cm^{-2}$)	N_f	R_{ct} ($K\Omega.cm^2$)	C_{dl} ($F.cm^{-2}$)	N_{dl}	R_p ($K\Omega.cm^2$)
30 min	0	18.08	1.5	2.1e-6	0.8	83.54	8.24e-6	0.3	85.04
60 min	0	20.43	0.03	13.7e-6	0.8	76.10	31.52e-6	0.3	76.13
30 min	2	20.50	8.1	17.9e-6	0.8	100.1	4.7e-6	0.2	108.2
60 min	2	20.99	3.5	9.3e-6	0.8	96.83	15.8e-6	0.5	100.33
30 min	4	18.57	0.07	29.6e-6	0.8	661.50	1.25e-6	0.4	661.57
60 min	4	10.48	43.1	36e-6	0.7	550	2.29e-6	0.1	593.1

Impedance studies were also carried out at open circuit potential (OCP) in (0.1M NaCl+ 0.1M H₂SO₄) solution for 60 min. annealed samples. In Nyquist plot, (Figure 43) similar capacitive depressed semi-circles were observed for all the samples from high to intermediate frequencies as was observed in 0.5M NaCl solution. However, the diameters of the loops were varying with the composition of the samples. Nyquist plot for sample with 4 wt. % Si consists of partial circle with indefinite radii and did not intersect X axis at any point. This behavior is related to highly capacitive character of passive materials. Same circuit as shown in Figure 37 was used to fit the curves and Echem analyst software used to acquire data. Table 10 shows summary of the data. The highest charge transfer resistance (R_{ct}) was observed in sample containing 4 wt.% Si (Fe-18Cr-4Si) which shows lowest susceptibility of the material in acidic chloride environment. Sample with 4 wt.% Si achieved the highest R_p value (415 KOhm.cm²) which further states that passive film formed has the highest protective ability.

Figure 43 shows combined impedance curves of 30& 60 min annealed sample in 0.1 M NaCl + 0.1M H₂SO₄. EIS spectra comparison of 30 and 60 minutes annealed samples revealed that the 60 minutes annealed sample with coarser grains size have less resistance to polarization as compared to the samples annealed for 30 minutes with relatively finer grain samples. The similar trend has been observed by Schino et al. [59] and Hua- Bing et al. [61] in their research. Finer gain size samples have more uniform and compact passive layer as compared to the coarse grained microstructure in which there is a more open passive layer. The better electrochemical properties observed in this research for finer grain size samples can be linked to the compact passive layer which has formed when the samples comes in contact with the chloride and acidic chloride

environments. The passive film compactness in the finer grain size samples can be linked with the grain boundary density which is more in finer grain samples as compared to the coarser grains sample. The high grain boundary density samples will achieve passivity more readily and this makes diffusion of the corrosive ions difficult in the passive film which in turns enhances electrochemical properties.

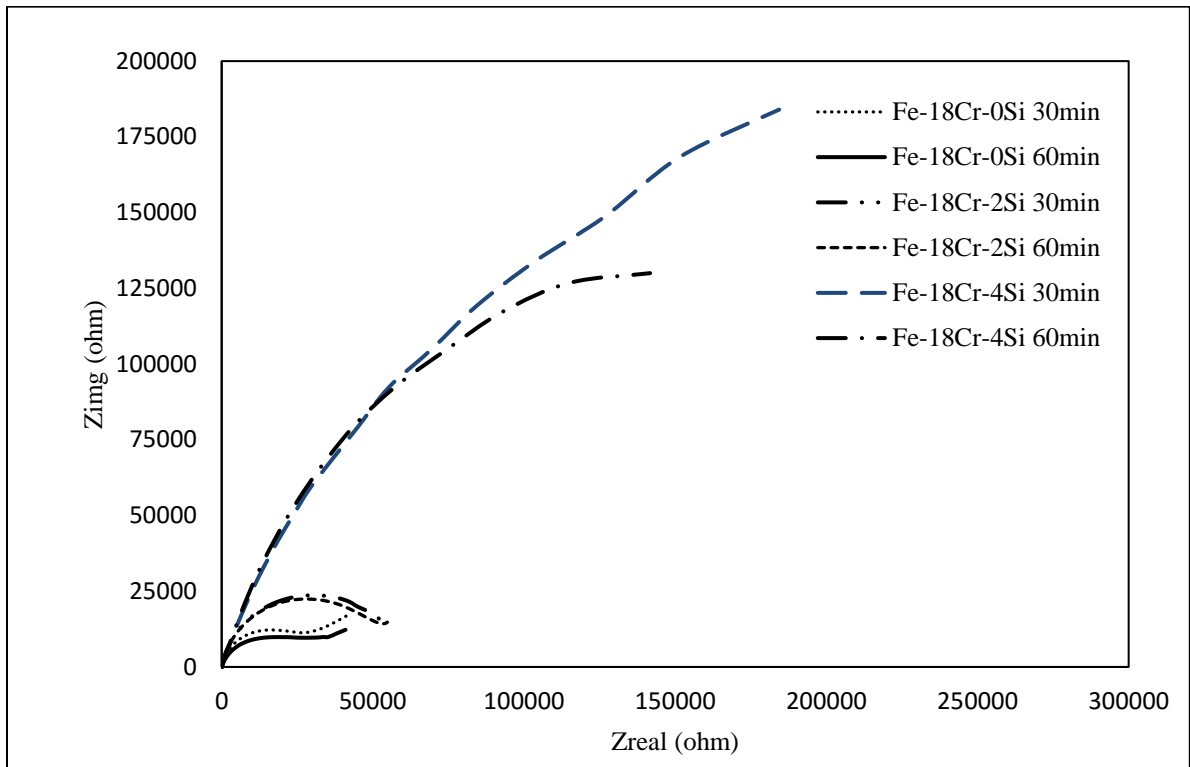


Figure 43: Combined Nyquist plot in 0.1M NaCl+ 0.1M H₂SO₄ solution for 30 and 60 min. annealed samples

Table 10: Combined EIS parameters obtained in 0.1M NaCl+0.1M H₂SO₄ solution for 30 & 60 min. annealed samples after curve fitting

Annealing Time	Si (%)	R_s (Ω.cm²)	R_f (KΩ.cm²)	CPE_f (F.cm⁻²)	N_f	R_{ct} (KΩ.cm²)	C_{dl} (F.cm⁻²)	N_{dl}	R_p (KOhm.cm²)
30 min	0	24.51	32.4	29.3e-6	0.8	21.35	63.5e-6	0.9	53.7
60 min	0	18.96	0.17	3.7e-6	1.0	35.88	26.08e-6	0.7	36.05
30 min	2	19.77	0.02	19.5e-6	0.8	58.1	0.9e-6	1.0	58.1
60 min	2	20.56	0.04	7.9e-6	0.9	58.63	13.1e-6	0.7	58.6
30 min	4	17.44	0.03	8.29e-6	0.7	581.5	3.95e-6	0.7	581.5
60 min	4	10.59	45.5	33.3e-6	0.8	370.0	4.52e-6	1.0	415.5

CHAPTER 6

CONCLUSIONS

The effect of silicon and grain size on electrochemical properties of Fe-18Cr-XSi alloy was studied by using different electrochemical techniques like Potentiodynamic polarization (PDP), Electrochemical Impedance Spectroscopy (EIS) and linear polarization methods (LPR).

The results showed that

- With an increase in silicon content, corrosion resistance of Fe-18Cr alloy measured in terms of i_{pass} & E_{pit} was improved in chloride (NaCl) solution. Alloy with 4% Si showed wider and stable passive range.
- In acidic chloride solution, increasing the silicon content in the alloy improves electrochemical properties like i_{pass} , i_{crit} and E_{pit} .
- Improved corrosion resistance of the alloy containing Si was attributed to the formation of a stable passive film at higher potentials
- Longer annealing time makes grains coarser due to which pitting resistance of the alloy decreased significantly
- Finer grain size sample were found to have positive effect on i_{crit} and i_{pass} in both chloride and acidic chloride solution as compared to the coarser grain size samples.

REFERENCES

1. Klar, E., Samal, P. Powder Metallurgy Stainless Steel, Processing, Microstructure, and Properties. (2007) ASM International.
2. H.H. Uhlig, *Corrosion Sci.* **1979**, *19*, 777.
3. N. Sato, *Corrosion Sci.* **1990**, *31*, 1.
4. A.Guntherschulze and H. Betz, *Z. Phys.* **1931**, *68*, 145.
5. Guntherschulze and H. Betz, *Z. Elektrochem.* **1931**, *37*, 726.
6. Guntherschulze and H. Betz, *Z. Phys.* **1934**, *92*, 367.
7. E.J.W. Verwey, *Physica*, **1935**, *2*, 1059.
8. N. Cabrera and N.F. Mott, *Rep. Progr. Phys.* **1948–1949**, *12*, 163.
9. F.P. Fehlner, and N.F. Mott, *Oxidat. Met.* **1970**, *2*, 59
10. Digby D. Macdonald, *Electrochimica Acta*, **2011**, *56*, 1761–1772
11. N. Cabrera and N.F. Mott, *Rep. Progr. Phys.* **1949**, *12*, 163–184
12. Leffler, B., *Avesta Sheffield AB Research Foundation, Stockholm, Sweden*, **1996**
13. A.L. Schaeffler and W.T. Delong, *Met. Prog.* **1949**, *56*, 680–688;
14. Raghavan V. *Phase diagrams of ternary iron alloys*, *ASM International* **1987**, *1*, 34
15. H. Fujikawa, T. Morimoto, Y. Nishiyama and S.B. Newcomb, *Oxid. Met.* **2003**, *59*, 23–40.
16. T. Oshima, T.Y. Habara and K. Kuroda, *Materials Science Forum*, **2007**, *539–543*, 4897–4902.
17. R. Pettersson, L. Liu and J. Sund, *Corr. Engg. Sci. Tech.* **2005**, *40*, 211–216.
18. G. Bamba, Y. Wouters, A. Galerie, F. Charlot and A. Dellali, *Acta Mater.* **2006**, *54*, 3917–3922.
19. F. Riffard, H. Buscail, E. Caudron, R. Cueff, C. Issartel and S. Perrier, *Mat. Charact.* **2002**, *49*, 55–65.
20. D. Itzhak and S. Harush, *Corr. Sci.* **1985**, *25*, 883
21. J. M. Blengino, M. Keddani, J. P. Labbe, and L. Robbiola, *Corr. Sci.*, **1995**, *37-4*, 621–643.

22. Wen-Ta Tsai, Y.-N. Wen, J.-T. Lee and H.-Y. Liou, *Surf. and Coat. Tech.* **1988**, *34*, 209 – 217
23. F. Velasco, A. Bautista and A. González-Centeno, *Corr. Sci.* **2009**, *51*, 21–27
24. R. Nishimura, K. Yamakawa , J. Ishiga , Y. Matsumoto and H. Nagano , *Mat. Chem. and Phy.* **1998**, *51*, 289-292
25. F.J. Pérez, M.P. Hierro, C. Gómez, L. Martínez and D. Duday, *Surf. and Coat. Tech.* **2000**, *133–134*, 344–350.
26. F.J. Pérez, M.P. Hierro, C. Gómez, L. Martínez and P.G. Viguri, *Surf. and Coat. Tech.* **2002**, *155*, 250–259
27. T.N. Rhodin. *Corr.* **1956**, *12-3*, 123-135
28. N.D. Thomasov, G.P. Chernova and O.N. Marcova, *Corr.* **1964**, *20-5*, 166.
29. O. Blajiev, L. Chigirinskaya and G. Chernova, *Electr. Acfa.*, **1998**, *43-1-2*, 199-202
30. I. I. Reformatskaya, I. G. Rodionova, A. N. PodobaeV, I. I. Ashcheulova and E. V. Trofimova. *Prot. of Met.*, **2006**, *42-6*, 549–554
31. Katsuya Hio, Takashi Adachi, Takashi Yamada and Yutaka Tsuchida. *Mat. And Trans.* **2001**, *42-8*, 1723 to 1730
32. J. M. Blengino, M. Keddani, J. P. Labbe, and L. Robbiola, *Corr. Sci.***1995**, *37-4*, 621–643,.
33. V. H. Radosevic, K. Kvastek, D. Hodko, and V. Pravdic, *Elect. Acta.***1994**, *39-1*,119–130
34. M. Gaberscek and S. Pejovnik. *Elect. Acta.*,**1996**, *41-7-8*, 1137–1142,
35. E. B. Castro and J. R. Vilche, *Elect. Acta*, **1993**, *38-11*, 1567–1572,
36. F. Mansfeld and H. Shih, *J. Elect.***1998**, *135*, 1171.
37. F. Mansfeld, *Electrochim. Acta* *35* (1990) 1533.
38. F. Mansfeld, S.H. Lin, S. Kim and H. Shih, *Corros. Sci.* **1987**, *27*, 997.
39. F. Mansfeld, S.H. Lin, S. Kim and H. Shih, *J. Electrochem.* **1990**, *137*, 78.
40. F.Mansfeld, Y. Wang, S.H. Lin, H. Xiao and H. Shih, *ASTM STP 1188, American Society for Testing and Materials, Philadelphia*, **1993**, 297.
41. J.R. Scully, R.P. Frankenthal, K.J. Hanson, D.J. Siconolfi and J.D. Sinclair, *J. Electrochem.* **1990**, *137*, 1365.

42. F. Mansfeld and B. Little, *Corros. Sci.* **1991**, 32, 247.
43. R. Oltra, M. Keddad, *Corros. Sci.* **1988**, 38, 1.
44. R. Oltra, M. Keddad, *Electrochim. Acta* **1990**, 35, 1619
45. C.C. Huang, W. Tsai and Ju-T. Lee, *Materials Science and Engineering*, **1995**, A190, 199-205
46. J.L. Polo, E. Cano, J.M. Bastidas, *Jour. of Electroanal. Chemi*, **2002**, 537, 183-187
47. C.H. Lin and J.G. Duh, *Surf. & Coat. Tech.* **2009**, 204, 784–787
48. E.O. Hall, *Proc. Phys.* **1951**, 64, 747.
49. N.J. Petch, *J. Iron Steel Inst.* **1953**, 174, 25
50. F. Forouzan, A. Kermanpur, A. Najafizadeh and A. Hedayati, *Int. J. Mod. Phys.* **2012**, 5, 383–390.
51. R. Song, D. Ponge, D. Raabe, J.G. Speer and D.K. Matlock, *Mater. Sci. Eng.* **2006**, 441, 1–17.
52. H.W. Zhang, Z.K. Hei, G. Liu, J. Lu and K. Lu, *Acta Mater.* **2003**, 51, 1871.
53. H.Q. Sun, Y.-N. Shi, M.-X. Zhang and K. Lu, *Acta Mater.* **2007**, 55, 975.
54. R.Z. Valiev, R.K. Islamgaliev and I.V. Alexandrov. *Prog. Mater. Sci.* **2000**, 45, 103.
55. R.Z. Valiev, T.G. Langdon, *Prog. Mater. Sci.* **2006**, 51, 881.
56. A. Di Schino, M. Barteri, J. Kenny and J. Mater. Sci. **2003**, 38, 3257–3262.
57. T. Balusamy, T.S.N. Sankara Narayanan, K. Ravichandran, I.S. Park and M.H. Lee, *Corr. Sci.* **2013**, 74 332–344.
58. L. Jinlong, L. Hongyun and *J.Nucl. Mater.* **2014**, 452, 469–473.
59. A. Di Schino, J. Kenny and *J. Mater. Sci.* **2002**, 21, 1969–1971.
60. L. Jinlong, L. Hongyun and *J.Mater. Eng. Perform.* **2014**, 23, 4223–4229.
61. H. Li , Z. Jiang , H. Feng , H. Zhu , B. Sun and Z. Li, *Int. J. Min. Met. Matrl.* **2013**, 20-9, 850.
62. Z.J. Zheng, Y. Gao, Y. Gui and M. Zhu, *Corros. Sci.* **2012**, 54, 60–67.
63. ASTM A763, *Standard Practices for Detecting Susceptibility to Intergranular Attack in Ferritic Stainless Steels* (2015)
64. ASTM E112, *Standard Test Methods for Determining Average Grain Size*

65. Verhoeven, J.D. *Fundamentals of Physical Metallurgy*, Wiley, New York, **1975**, 326
66. Cowan, R.L and Tedmon, Adv. Corr. Sci. and Tech. **1973**, 3 , 293
67. O. V. Kasparova, Yu. V. Baldokhin and M. O. Anosova, *Prot. of Met.* **2008**, 44, No. 6, 593–598
68. W.T. Tsai, Y.N. Wen, J.T. Lee, H.Y. Liou and W.F. Wang, *Surf. Coat. Tech.* **1988**, 34 209–217.
69. R. Robin, F. Miserque and V. Spagnol, *J. Nucl. Mater.* **2008**, 375, 65–71.
70. I.H. Toor, J. Kwon and H. Kwon, *J. Electrochem. Soc.* **2008**, 155, C495-C500.
71. C. Liu, Q. Bi, H. Ziegele, A. Leyland, A. Matthews and J. Vac. *Sci. Technol.* **2002**, A 20 (3) 772.
72. U. Rammelt and G. Reinhard, *Corros. Sci.* **1987**, 4, 373–382.
73. N.E. Hakiki, M.F. Montemor, M.G.S. Ferreira and M.D. Cunha Belo, *Corros. Sci.* **2000**, 42, 687-702.
74. M.F. Montemor, M.G.S. Ferreira, N.E. Hakiki and M. Da Cunha Belo, *Corros. Sci.* **2000**, 42, 1635
75. N.J. Medvedeva, Y.N. Gornostyrev, D.L. Novikov, O.N. Myrasov and A.J. Freeman, *Acta Metall. Mater.* **1998**, 46, 3433-23.
76. Y.L. Zhou, M. Ninomi, T. Akahori, H. Fukui and H. Toda, *Mat. Science. Eng.*, **2005**, 398A, 28.
77. R. A. R. Díaz, J. U. Chavarín1, A. M. Ocampo, J. P. Calderón, M. G. Pérez2, J.M. L. Oglesby, J. G. G.Rodríguez and J. A. J. Islas *Int. J. Electrochem. Sci.*, **2013**, 8, 958 - 972
78. E. E. Oguzie, J.Li , Y. Liu, D. Chen, Y. Li, K. Yang and F. Wang, *Electrochimica Acta*, **2010**, 55, 5028–5035
79. D. Wallinder, J. Pan, C. Leygraf and D.Bauer, *Corros. Sci.* **1998**, 41, 275–289.
80. L. Jinlong, *J. Mater. Sci. Technol.* **2017**
81. L. Jinlong, *Mat. Sci. and Eng. C.*, **2016**, 62, 558–563
82. T. Balusamy, S. Kumar, T.S.N. S. Narayanan; *Corr. Sci.* **2010**, 52, 3826–3834

Vitae

Name : Nabeel Ameer

Nationality : Pakistan

Date of Birth : 04/04/1988

Email : nabeeluet06@gmail.com.

Address : House No MCB 7/138 Masjid Khuwajgan, Mohalla
Janjua Street Chakwal, Pakistan

Academic Background : I have completed my Bachelors in Metallurgical and Materials Engineering from University of Engineering & Technology Lahore, Pakistan in 2010. After that In September 2011, I was enrolled in Master degree program at King Fahd University of Petroleum & Mineral in the field of Material Science and Engineering as a part time student. I took several courses such as Advanced Corrosion, Material Characterization, Material Structure and defects and Corrosion in oil and petrochemical industries which helped me to accomplish my thesis work. During my master's studies, I joined a multinational company "Exova" as a failure analyst in which my job responsibly was to conduct failure investigation / root cause analysis on failed components from oil and gas industry. |